High Speed Videography of Welding — Part 2: Applications with Front- and Backlighting

A discussion of the front- and backlighting techniques and equipment needed and applying those concepts in concrete welding conditions

BY S. D. GUEST, G. GÖTT, G. DAPP, J. CHAPUIS, AND P. F. MENDEZ

Abstract

This paper is the second of a three-part series covering the field of high-speed videography in welding. This second part provides a comprehensive discussion of two of the most common techniques of high-speed imaging of welding: backlighting and frontlighting, including broad and narrow-spectrum lighting (lasers in the case of backlighting) with both techniques. In all cases, building on the foundations laid out in Part 1, detailed descriptions of appropriate setups are provided together with examples of published practical implementations. The welding processes addressed include laser beam welding, gas tungsten arc welding, gas metal arc welding (GMAW), flux cored arc welding, and submerged arc welding. The advantages and disadvantages of front- and backlighting are explored in detail. Frontlighting is especially useful for processes with high dynamic range, such as short-circuit metal transfer in GMAW. Backlighting is less used with modern digital cameras; however, small amounts of backlighting can highlight features such as the electrode extension when using natural radiation lighting. Narrow-spectrum sources such as lasers are especially useful in combination with narrow bandpass filters to eliminate unwanted radiation sources. The implementations of front- and backlighting reviewed in this paper, together with those for natural radiation lighting in Part 3 and the fundamental concepts and resulting quantitative guidelines provided in Part 1, provide welding researchers with a previously inexistent compilation of criteria to select proper equipment, accessories, and parameters for high-speed imaging of a vast variety of phenomena in welding, laser welding, and associated processes such as additive manufacturing or cutting.

Keywords

- Metal Transfer
- Laser Lighting
- Reflected Light
- Imaging

Introduction

Part 1 of this work established the scientific and technological foundations of high-speed videography of welding operations, including considerations of time scales, emissions of light from the welding operation, and considerations of sensors, lenses, filters, and software. The concepts, terminology, and acronyms used in this paper were also explained in detail in Part 1.

This paper focuses on applying those fundamental concepts in concrete welding conditions. The survey is organized according to the method of adding or collecting light during imaging, dramatically impacting video quality. Lighting techniques in the literature are surveyed exhaustively and discussed in detail. Typical setups for the different techniques are described, and image examples are presented, sourced from both literature and the authors.

The techniques for lighting high-speed videography of welding can be divided into three categories: backlight, frontlight, and natural radiation, as shown schematically in Fig. 1. Each of these techniques is described in detail with extensive examples from both the literature (with the appropriate citations) and those specifically developed for this paper. Natural radiation will be addressed in detail in Part 3.

https://doi.org/10.29391/2026.105.003

Backlighting

Backlighting is a common technique that creates shadow images in which the electrode, metal droplets, and weld pool surface appear dark against a light background, providing a clear image of free surface contours. Backlighting is best when the backlight source's wavelength is selected to avoid spectral line peaks of the welding arc constituents and is of sufficient power to overcome the emitted arc and molten metal radiation.

Backlighting commonly uses a visible light source (preferably monochromatic) or a laser in near-IR wavelengths to overpower the arc and metal emissions. A filter, typically a narrow bandpass (NBP) with a transmitting wavelength similar to the backlight source, eliminates the welding arc and metal spectral lines.

Backlighting has some limitations, such as providing no information about the plasma or radiative emissions from the molten metal (which relate to droplet temperature). Observing or discriminating surface texture, slags, or oxides on the molten metal's surface is also impossible.

Broad Spectrum Backlighting

Common tools for backlighting systems include halogen, light-emitting diode (LED), xenon, and metal halide lamps. They emit light from the ultraviolet to infrared wavelengths and contain several spectral peaks within the visible light spectrum, allowing for the use of cameras without IR sensitivity. These lighting systems are available in high power outputs, and multiple light sources can be used simultaneously. While relatively inexpensive and available in high

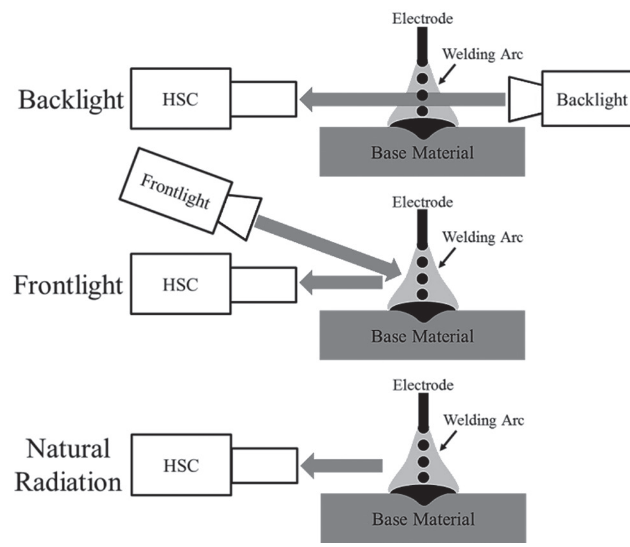

Fig. 1 — Setup for backlighting, frontlighting, and natural radiation lighting techniques.

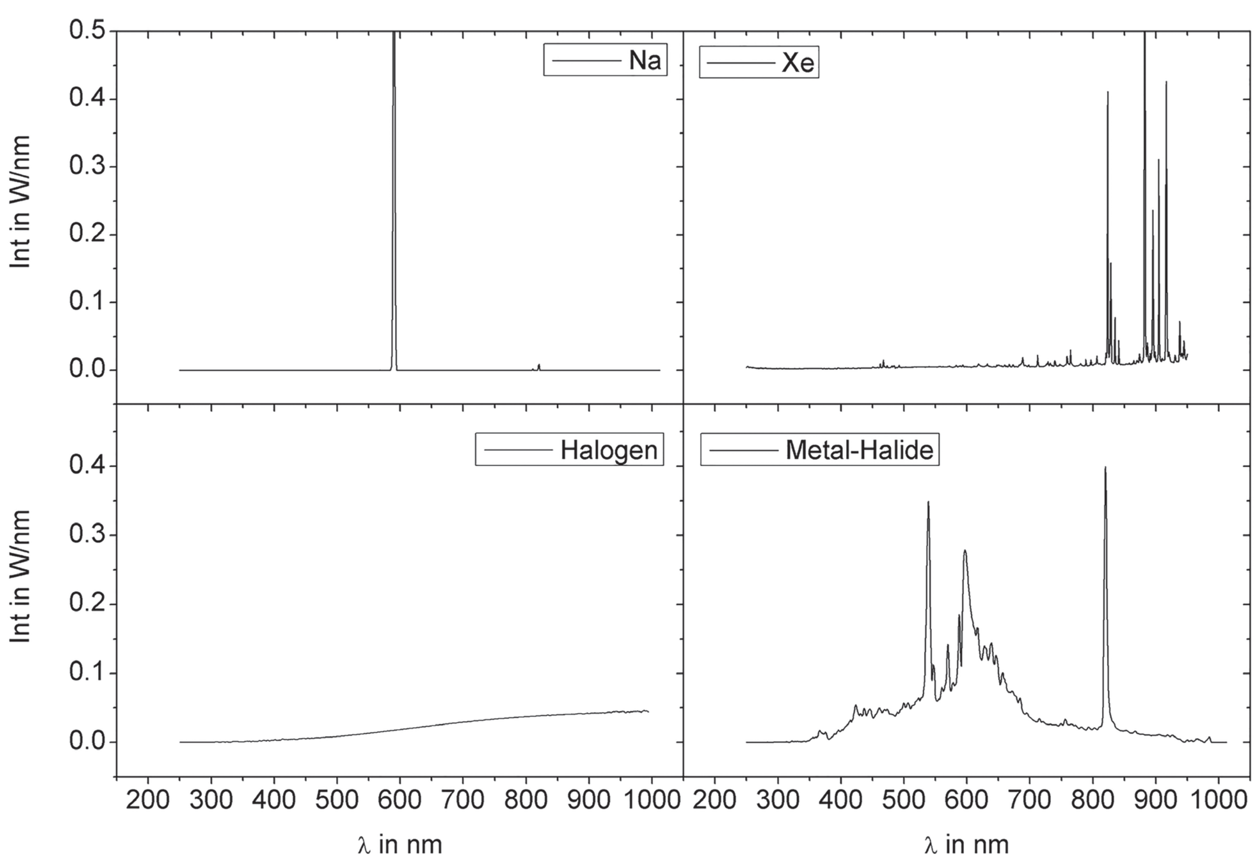

Fig. 2 — Spectra of backlighting sources.

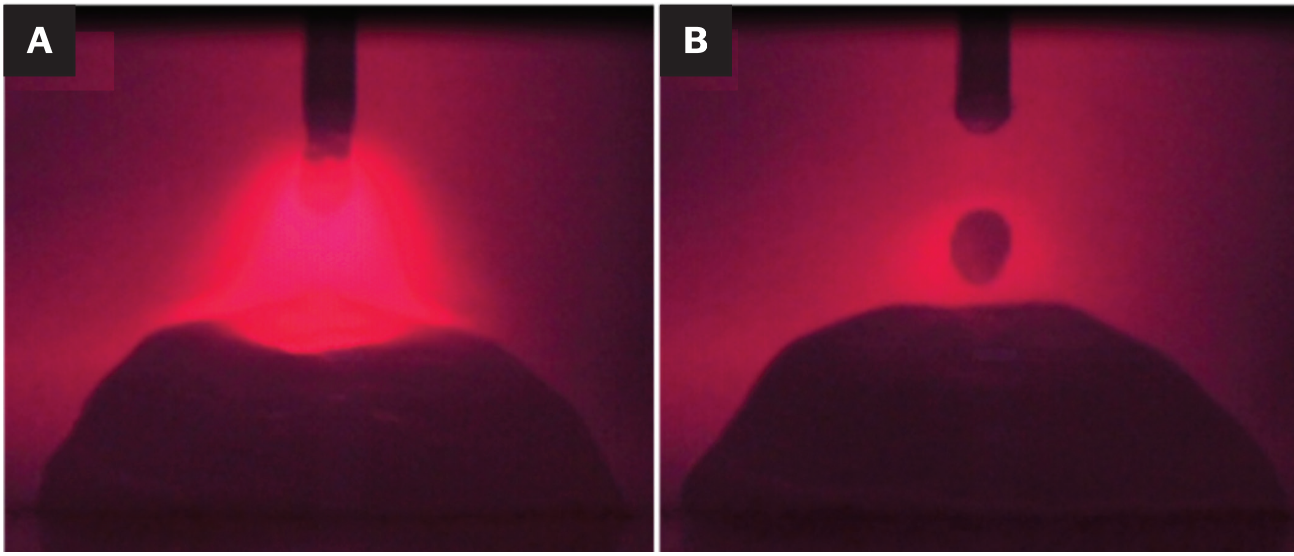

Fig. 3 — Backlighting of mild steel pulsed GMAW using a 250 W halogen source and a 650 ± 10 nm NBP filter. (Refs. 1, 2).

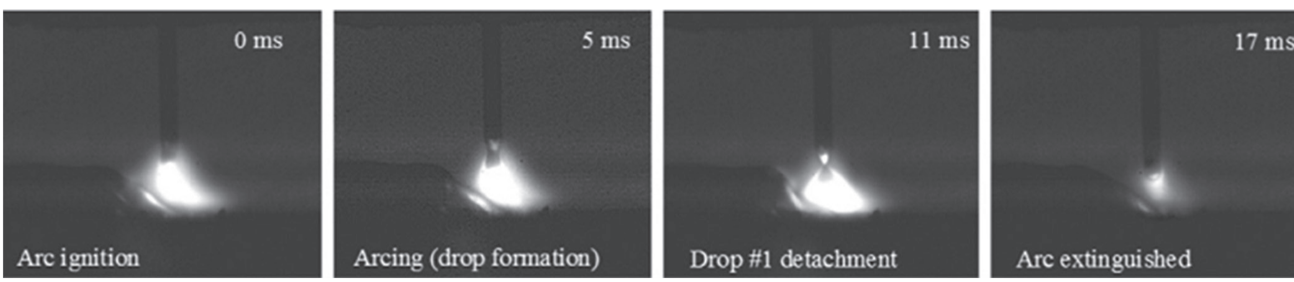

Fig. 4 — Backlighting of controlled short-circuit GMAW of 4043 aluminum in pure Ar using a 60 W, 530 nm green LED source and with a 60 W green LED with a 530 ± 10 nm NBP filter (Ref. 7).

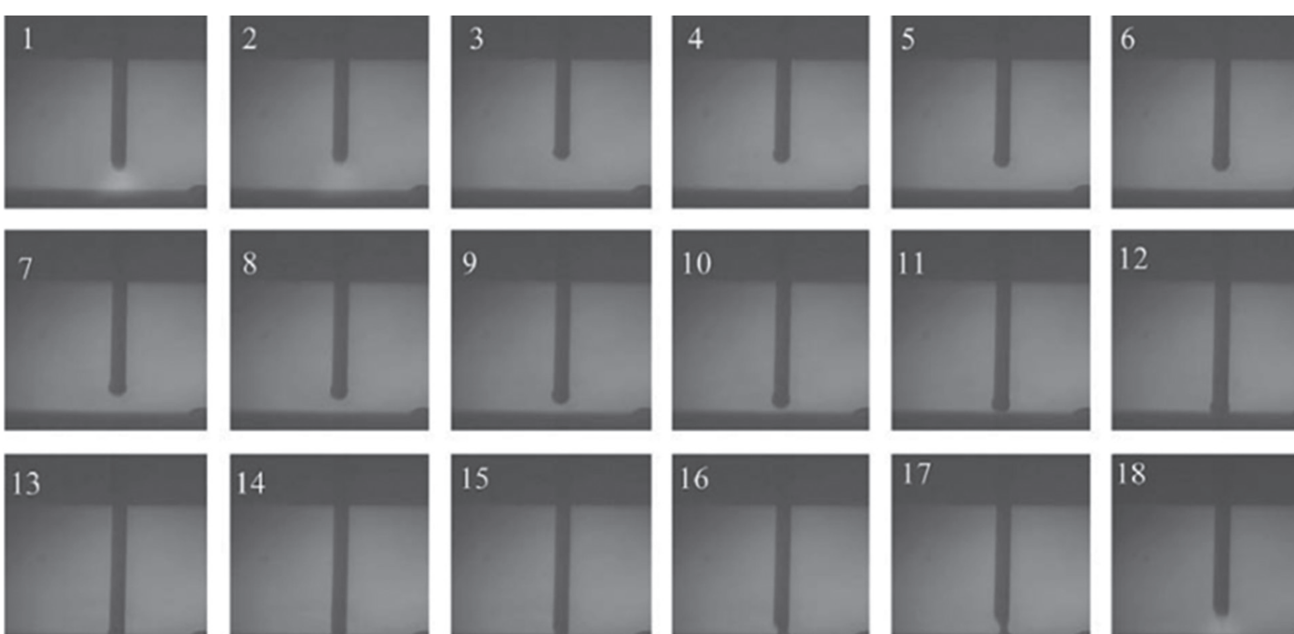

Fig. 5 — Xenon backlighting of GMAW aluminum-controlled short-circuit (Fronius CMT) with pure argon shielding gas (Ref. 14).

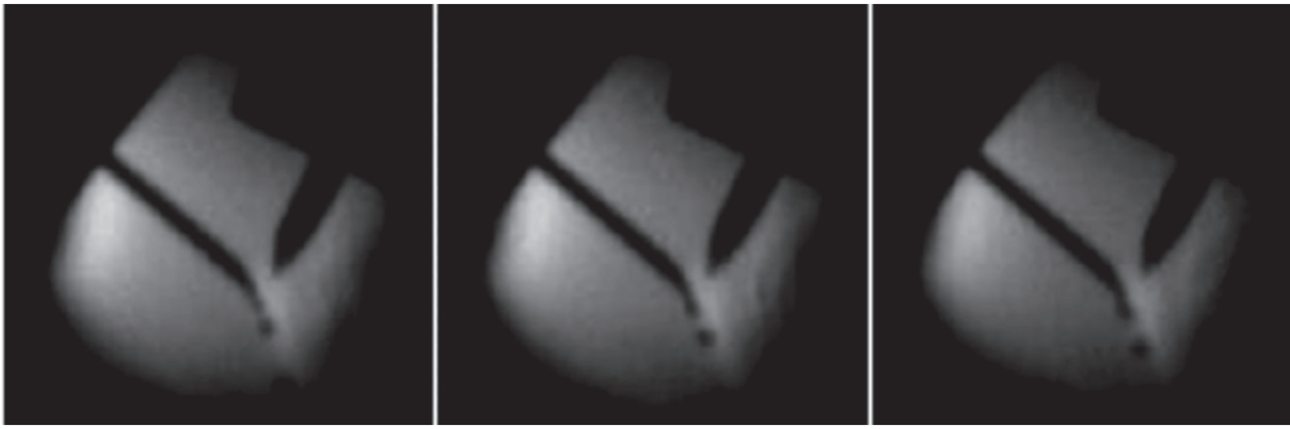

Fig. 6 — Xenon backlighting of a GMAW of CuSi3 in free-flight assisted with a GTAW arc in pure argon shielding gas (Ref. 15).

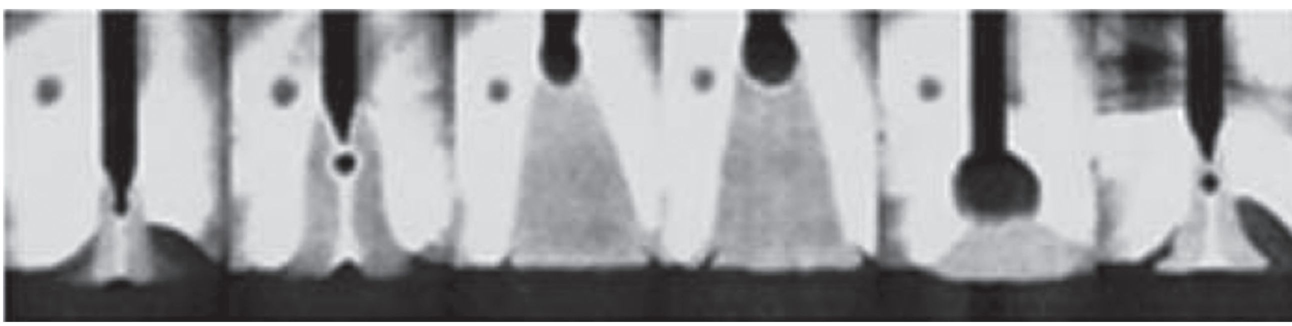

Fig. 7 — Mercury vapor backlighting of a GMAW of mild steel in free-flight at approximately 200 A in pure argon shielding gas (Ref. 17).

power outputs (above 100 W), their relatively broad spectrum can result in low power outputs at specific spectral lines of interest, hindering the complete elimination of the arc and limiting the maximum frame rate possible, as the images can be underexposed.

Setup for Visible Light Backlighting

The experimental setup required for visible light backlighting is straightforward and inexpensive. The light source is placed opposite the camera to direct the most light through the welding arc and metal droplets. Most light sources feature a bulb placed inside a reflector to direct the light over a much larger area than the welding region of interest. Collimating the light to a single small beam increases the intensity of light directed toward the welding region, overpowering the arc and producing clearly contoured videos. Halogen, LED, xenon, and metal-halide light sources emit a wide spectrum of light with characteristic spectral peaks of higher intensity. The light source selected must emit most of its light where there are no spectral lines of the arc, and a narrow bandpass filter with transmittance at the wavelength of the light source is typically used for optimal results.

Figure 2 illustrates measurements done for this work at the research institute INP Greifswald, showing the spectra of four common light sources; the vertical axes show the intensity of spectral flux in W/nm. The sodium lamp stands out for its monochromatic yellow light and is ideally suited for backlight imaging. Conversely, a halogen light source has a broad and smooth spectrum that is not especially strong at any wavelength; thus, it overlaps with the arc light, resulting in lower quality images. The xenon lamp shows multiple lines, and the metal halide lamp shows continuum and line spectra characteristics.

The cost of a visible light backlighting system can vary depending on the desired power outputs and frame rates; however, the total system cost at publication was typically less than $1500.

In a welding lab, there are usually different power sources available. A cheap light source that can be improvised would be any welding arc, such as a gas tungsten arc welding (GTAW) arc. The disadvantage is that the wavelength emitted by this arc might overlap with the wavelengths from the arc that needs to be observed. One way to overcome this limitation is to operate the illuminating GTAW arc at high powers to generate different illumination wavelengths.

Examples of Welding Imaging Using Visible Light Backlighting

Halogen backlighting is perhaps the most available and inexpensive lighting source for welding videography.

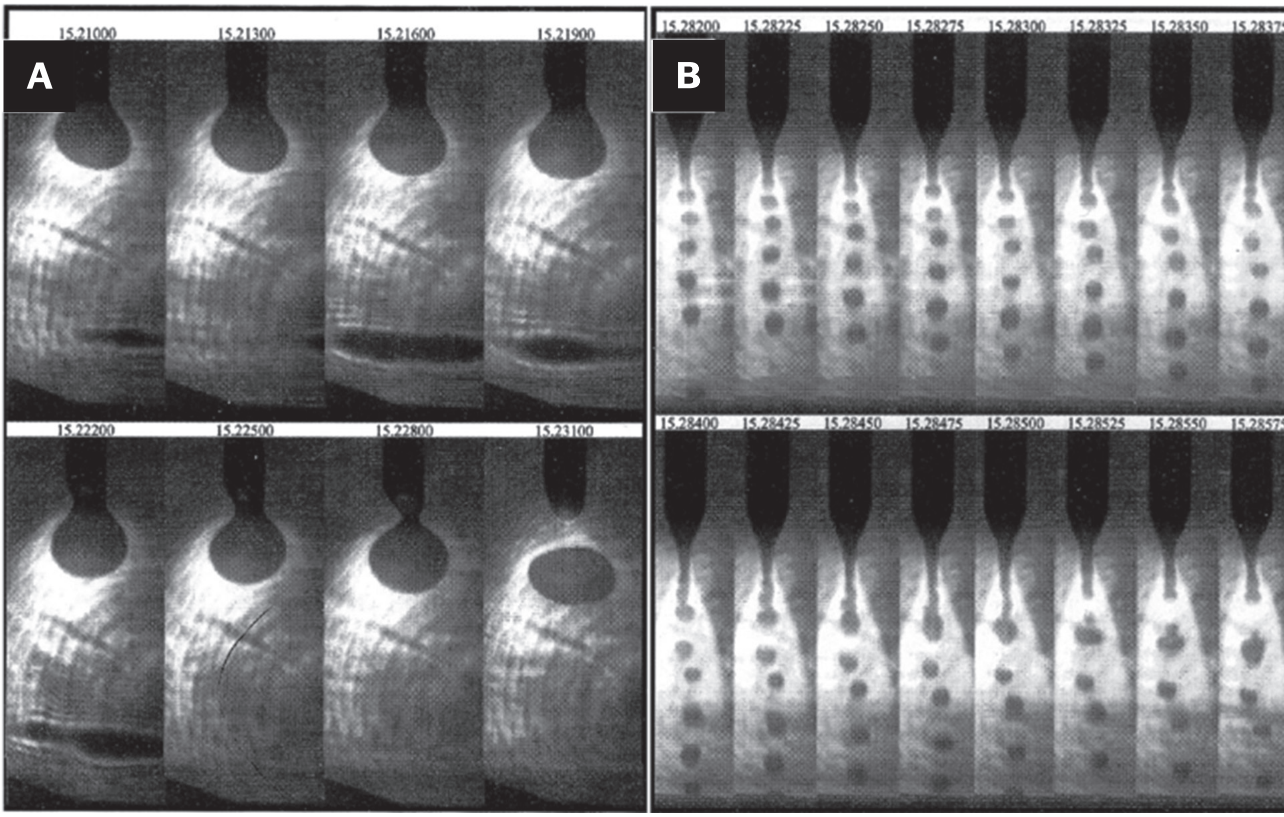

Fig. 8 — He-Ne laser backlighting with a 2 mW laser and NBP filter of GMAW of mild steel in free-flight mode in Ar-2% O_2 (Ref. 17): A — Globular; B — Spray.

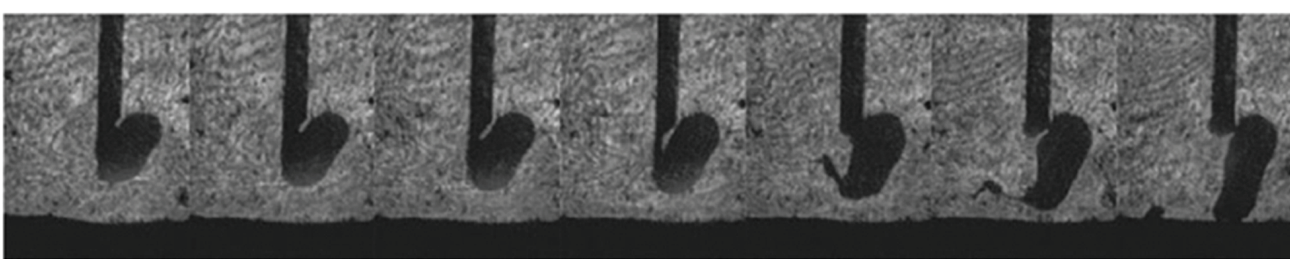

Fig. 9 — He-Ne laser backlighting of GMAW of mild steel in globular transfer in Ar-35%CO_2 (Ref. 37).

Figure 3 shows a typical halogen backlit image of pulsed gas metal arc welding (GMAW) using a 250 W light source, a color camera, and a 650 ± 10 nm bandpass (BP) filter situated in the red color of the visible spectrum (Refs. 1, 2). In these images, the high arc current of the pulse saturates the camera sensor and loses definition of the droplet and weld pool surface. In contrast, the lower background current does not overpower the halogen backlight and provides appropriate shadowgraph images.

Increasing the halogen power and using a neutral density filter or faster exposure would reduce the sensor saturation due to the arc during the peak pulse while retaining features of the weld pool and molten droplets during both the peak and background current stages. Another option would have been to replace the 650 ± 10 nm BP filter, chosen to avoid most of the strong metal (350600 nm) and gas lines (700–850 nm). The downside is that it records only a narrow spectral range of the continuum light source. Therefore, most of the lighting power is lost, and the strong lines from the arc overpower it in the high current phase. A long-wave pass filter at around 900 nm would integrate over a broader spectral range of the halogen lamp, use more of its power output, and still avoid most of the spectral lines of the arc.

Nakamura et al. studied the effect of shielding gas on metal transfer stabilization in experimental multilayer solid GMAW wires using a halogen backlight (Refs. 3, 4). Wong and Ling also used a halogen light source coupled with a bandpass filter to study the effect of shielding gas on metal transfer in steel GMAW (Ref. 5).

Light-emitting diodes provide a cost-effective and low-power consumption backlighting system. Figure 4 shows an example of controlled short-circuit GMAW (Fronius CMT) of 4043 aluminum in pure Ar illuminated with a 530 nm, 60 W green LED with a 530 ± 10 nm NBP filter. Backlight-

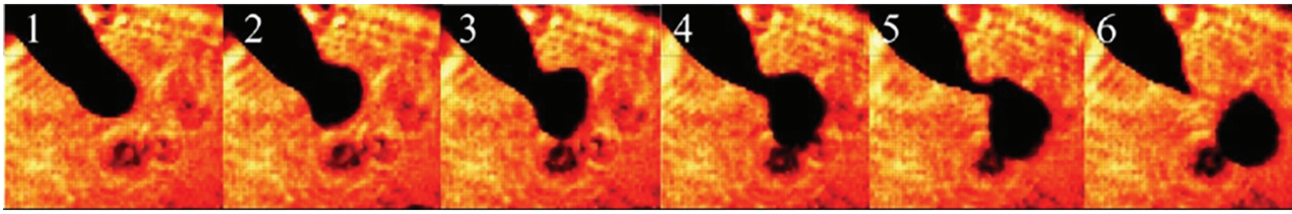

Fig. 10 — Laser backlighting with a 100 mW 650 nm laser and NBP filter of 650 nm ± 1.5 nm of GMAW of mild steel in pulsed mode in Ar-20%CO2. Images correspond to a 540 A pulse (Ref. 44) steel in pulsed mode in Ar-20%CO_2. Images correspond to a 540 A pulse (Ref. 44).

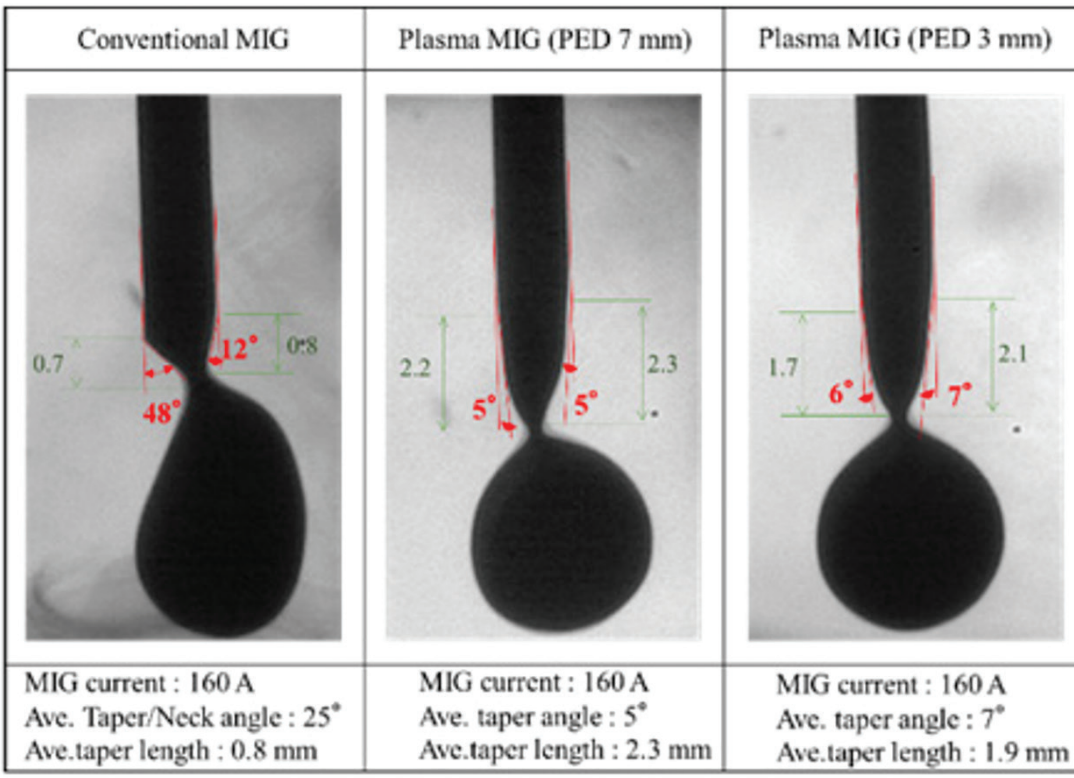

Fig. 11 — Laser backlighting with a high-power 640 nm laser and a 640 nm BP filter plus ND on the camera of GMAW and plasma GMAW (Ref. 45).

ing with lasers can also enhance natural radiation lighting videos (Ref. 6), for example, to better see the unmelted wire, which is unclear in Fig. 4.

Xenon backlighting is similar to halogen light sources and can produce excellent results due to its higher intensity and higher color temperature. Xenon has been used in aluminum and steel GMAW, steel flux cored arc welding (FCAW), and hybrid GTAW-assisted GMAW welding and brazing processes (Refs. 8–13). Figures 5 and 6 depict typical metal transfer images utilizing a xenon backlight. Unfortunately, the references do not specify the filter properties or whether filters were used at all. Figure 5 shows xenon backlighting of GMAW of aluminum controlled short-circuit (Fronius CMT) transfer mode with pure argon shielding gas (Ref. 14). Figure 6 shows xenon backlighting of a GMAW of CuSi3 in free-flight metal transfer mode assisted with a GTAW arc in pure argon shielding gas (Ref. 15).

Metal-halide light sources operate similarly to halogen and xenon lamps (Refs. 16–18). Figure 7 contains images of free-flight GMAW taken with a mercury vapor backlight.

Laser Backlighting

Laser backlighting works on the same principle as visible light sources. However, key differences exist. Lasers concentrate their light in a narrow spectrum around a nominal wavelength, resulting in a very intense light source that can easily overpower the welding arc at the laser wavelength, in contrast to halogen/xenon/metal halide light sources with broader light spectra or multiple peaks. Lasers are available in various wavelengths, from visible light (e.g., red or green lasers) to near-infrared wavelengths. The choice of laser wavelength must be within the spectral sensitivity of the high-speed camera sensor and must avoid the wave-

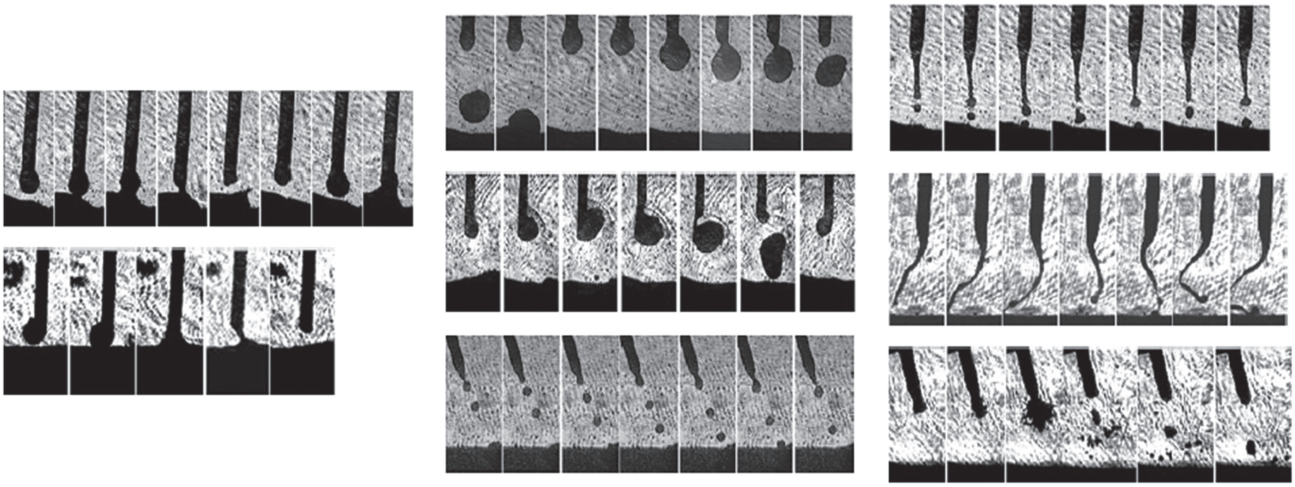

Fig. 12 — Schlieren patterns in the overview of metal transfer modes using 2000 fps and 632.2 nm He-Ne backlighting (Ref. 28).

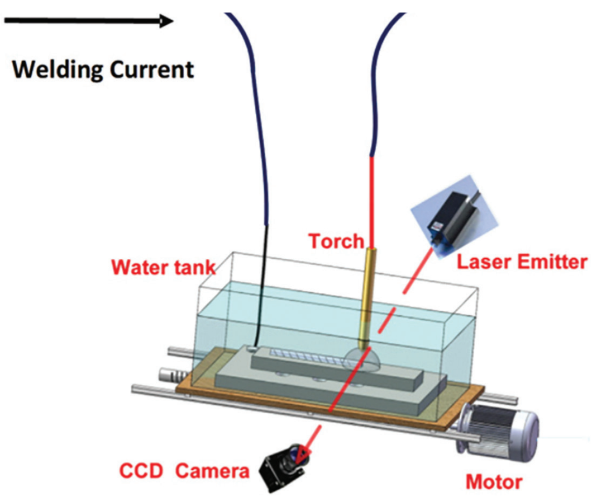

Fig. 13 — Underwater welding laser backlighting system used in Ref. 53.

lengths of arc emissions as much as possible. Since lasers are monochromatic, they generate self-interference, which can be seen as "laser speckle." This effect is visible in many examples, except when the background is overexposed.

Setup for Laser Backlighting

The laser backlighting equipment setup is similar to all other backlighting, with the laser placed opposite the high-speed camera and the beam directed through the welding arc. Lasers are available with different beam diameters and often require laser-specific optics to best visualize the weld pool and metal transfer. Depending on the laser beam's wavelength, collimating or dilating it can be difficult and can impact the total laser backlighting system cost. The cost of a laser system increases with power output and shorter wavelengths; visible lasers cost more than near-IR at equivalent power outputs. Laser backlighting does not require powerful lasers, often less than 1000 mW, as most laser power is projected at the primary specified wavelength. At the time of publication, typical laser backlighting systems cost less than $2000, including laser, power supply, optics, and NBP filter.

Because of the narrow spectrum of emission of lasers, they are ideally suited to be used with NBP filters of the same wavelength. When the laser wavelength avoids major spectral peaks of the welding arc and molten metal, the required laser power can be much lower than other light sources of broad spectrum, enabling the use of inexpensive continuous wave lasers (i.e., not pulsed) down to 2 mW. The shadowgraph image can be projected and focused on the camera sensor itself or onto a frosted pane of glass, as demonstrated by Soderstrom (Ref. 19).

Examples of Welding Imaging Using Laser Backlighting

The earliest use of laser backlighting involved He-Ne lasers with a visible light wavelength of 633 nm and a narrow full width half maximum, enabling good spectral responses when using film and early charge coupled device sensors. Allemand et al. built an early 2 mW He-Ne backlight system, including an NBP filter for studying metal transfer (Ref. 20). Zhang et al, Subramaniam et al., Soderstrom et al., and Jones et al., using the system outlined by Allemand et al., conducted thorough studies on GMAW metal transfer (Refs. 21–27) using He-Ne lasers. Scotti et al. used a He-Ne laser setup to provide an overview of various transfer modes in (Refs. 28, 29). Subramaniam et al. studied the effect of pulsing parameters on droplet size in pure argon-shielded GMAW with 4047 Al filler wire (Ref. 24). Soderstrom et al. validated the free-flight metal transfer mode during droplet calorimetry and characterized the metal transfer in Ar-CO_2 shielded GMAW with steel wires as thin as 0.4 mm (Refs. 25, 30). Jones et al. studied the steel GMAW free-flight transition from globular to spray metal transfer in Ar-2%O_2 (Ref. 31). Figure 8 contains sample images from Jones et al. during globular and spray metal transfer, showing good discrimination of the metal droplets from the welding arc.

The He-Ne laser backlighting system is very versatile, resulting in high uptake in research for metal transfer characterization. Yuan-Mei et al. and Rhee and Kannatey-Asibou used a He-Ne laser backlight to study metal transfer in GMAW (Refs. 32, 33). Balsamo et al. designed a synchronized data acquisition system for simultaneous collection of current and voltage signals with a 20mW He-Ne laser backlight with an NBP filter for metal transfer characterization (Ref. 34). Scotti et al. used the same system outlined by Balsamo et al. for analyzing the momentum of metal droplets in aluminum GMAW and the effect of out-of-phase pulsing on metal transfer in twin-wire GMAW (Refs. 35, 36). Figure 9 contains sample images from Alves de Resende et al., who studied the effect of CO_2 and O_2 on globular metal transfer in Ar-based shielding gas (Ref. 37).

The wide range of laser wavelengths has enabled researchers to work in different wavelength regimes (Refs. 38–43). Mota et al. and Abdullah et al. described the design of an inexpensive lighting system that includes synchronization drivers utilizing 905 nm laser diodes (Refs. 38, 40, and 43). Zhang et al. used a 100 mW 650 nm laser with a 650 ± 1.5 nm NBP filter to analyze metal transfer in pulsed GMAW and laser-hybrid GMAW, shown in Fig. 10 (Ref. 44).

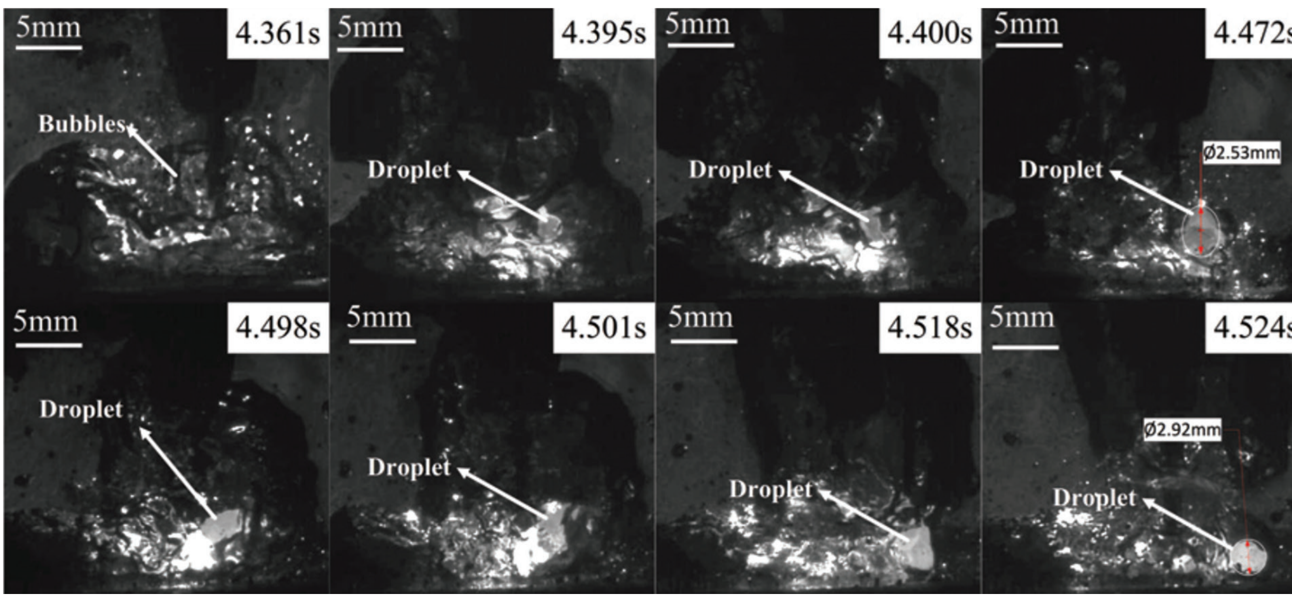

Fig. 14 — Laser backlighting imaging of repelled globular transfer in pulsed underwater FCAW (Ref. 53). The camera had a CCD sensor at a frame rate of 2000 fps; the laser wavelength and power were not specified.

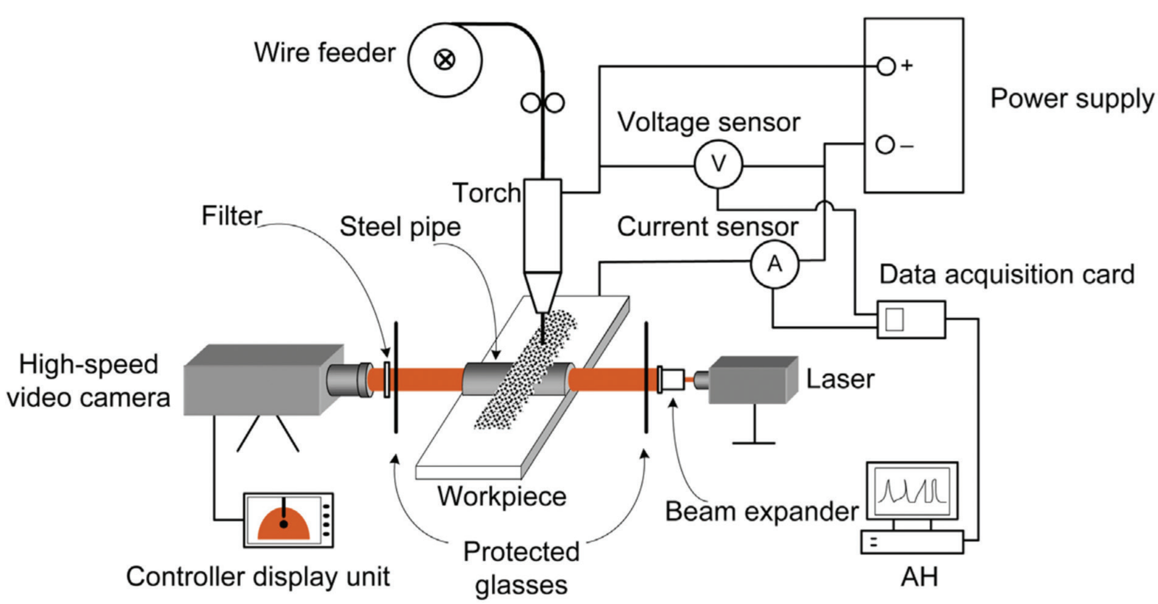

Fig. 15 — Experimental setup for laser backlighting to capture metal transfer in SAW (Ref. 54).

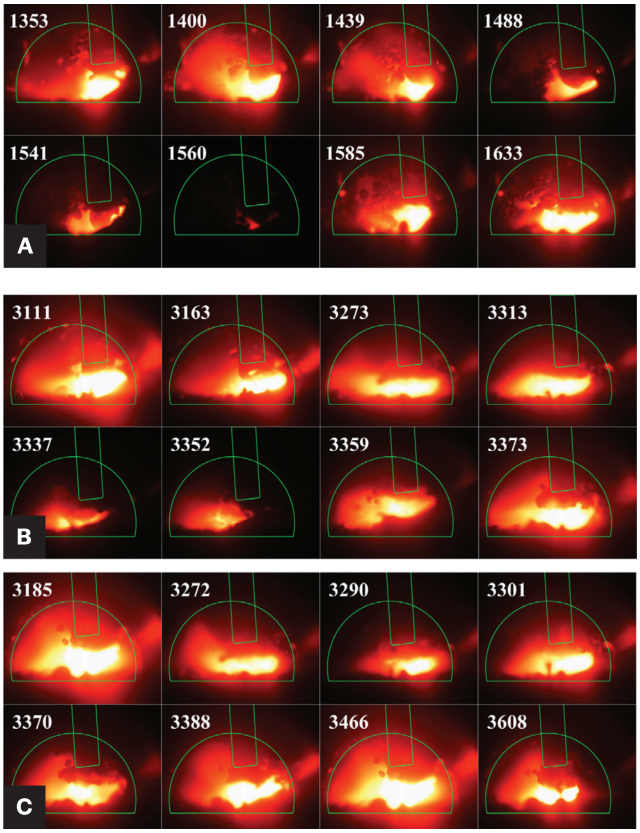

Fig. 16 — Laser backlighting of metal transfer in SAW at: A — 29 V 414 A; B — 35 V 495 A; C — 45 V 588 A (Ref. 54).

Mamat et al. used a high-power CAVILUX™ HF system (Cavitar) with a 640 nm wavelength pulsed diode emitter to visualize the taper formation in metal transfer for a plasma GMAW setup (Ref. 45). In conjunction with a 640 nm BP filter plus a neutral density (ND) filter on the camera, they overpowered the arc emissions and obtained the images shown in Fig. 11.

In most laser backlighting systems, the narrow spectrum produces the laser speckle effect mentioned in the section "Laser Backlighting." Another visual effect is the "streaking" effect, which occurs in connection with small point-shaped light sources that radiate through a nonisothermal gas or plasma. The variation in temperature means a variation in the refractive index. This creates an irregular pattern of diffuse light and dark lines outside the shadow of the metal. These patterns are clearly visible, for instance, in the overview of metal transfer modes provided in Fig. 12. These "schlieren" patterns are affected by the motion of the gas and contain information about the fluid mechanics of the plasma. This type of analysis of the plasma during metal transfer is still in its early stages, and limited publications exist (Refs. 46–51).

A special case of laser backlighting was demonstrated in Refs. 52 and 53 for imaging the metal transfer in underwater FCAW. This setup moved a water tank containing the substrate through the optical path between a stationary torch, a high-speed camera, and a laser emitter (see Fig. 13). The laser illumination used the principles of laser backlighting to reveal visual details such as arc length and droplet shape inside the bubble (see Fig. 14), which otherwise are difficult to capture underwater.

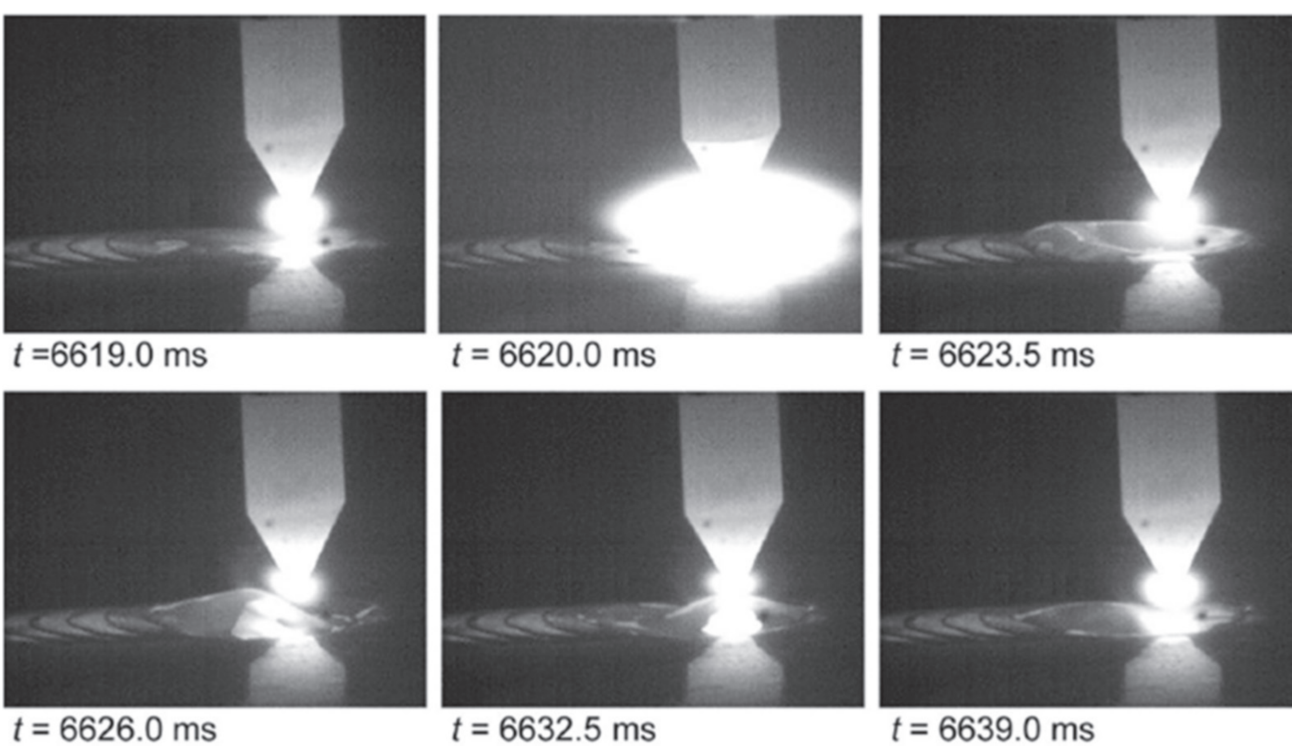

Fig. 17 — Frontlighting with a 150 W halogen source of pulsed autogenous GTAW of AISI 316L stainless steel in Ar-5%H_2 for determining weld pool oscillation frequency. Peak current is 300 A and background current is 47 A (Ref. 55).

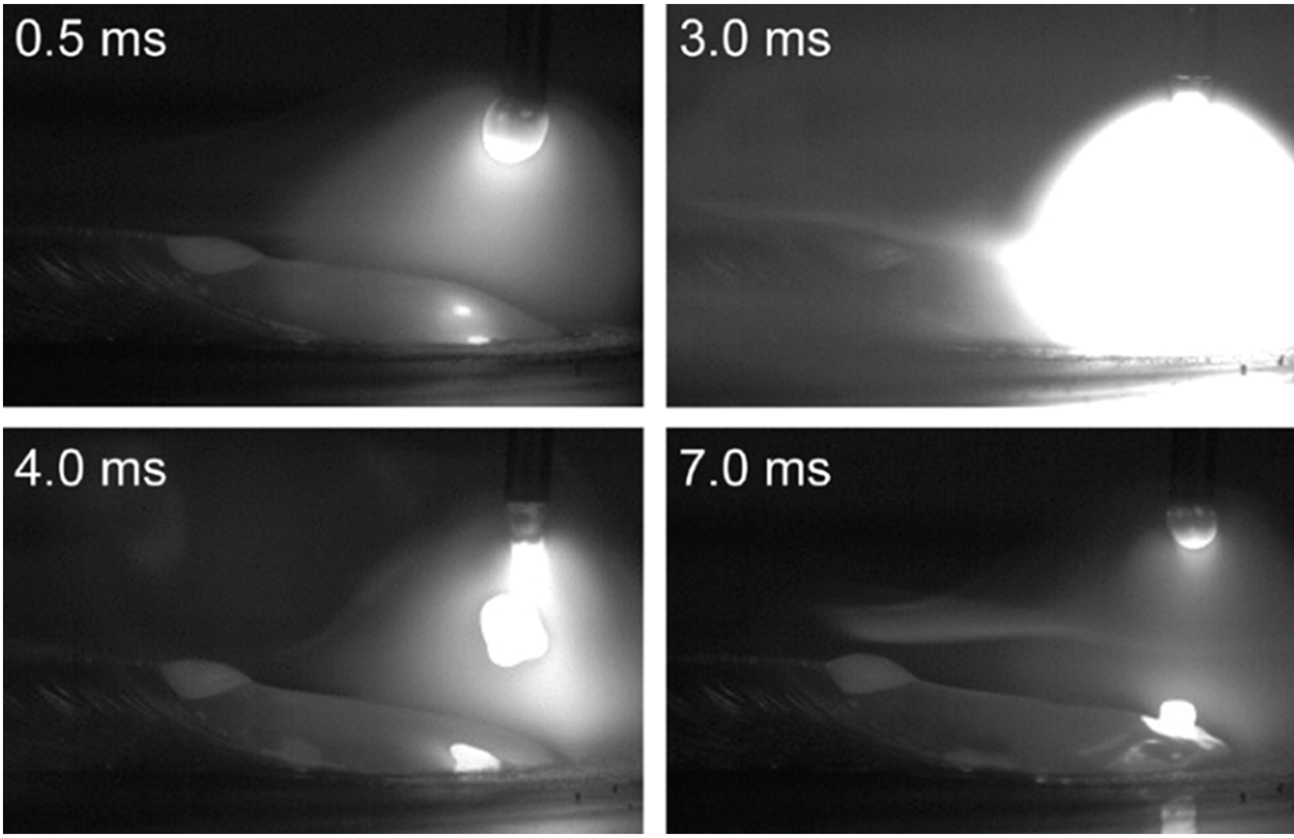

Fig. 18 — Frontlighting with a 2000 W halogen source of pulsed GMAW of ER70S-6 in Ar-5%CO_2 for determining weld pool oscillation frequency. Peak current is 290 A and background current is 58 A (Ref. 55).

Li et al. (Ref. 54) used a 300 mW, 650 nm laser as a backlight to capture metal transfer in submerged arc welding (SAW) (Fig. 15). A section of stainless steel pipe was placed perpendicular to the welding direction to create an opening into the flux. The authors captured the images at a relatively low frame rate of 2000 frames per second (fps). As a result of the intense activity and interaction of arc, fluxes, molten metal, and slag, especially at higher currents, the metal transfer was not imaged as clearly as in other welding processes (Fig. 16).

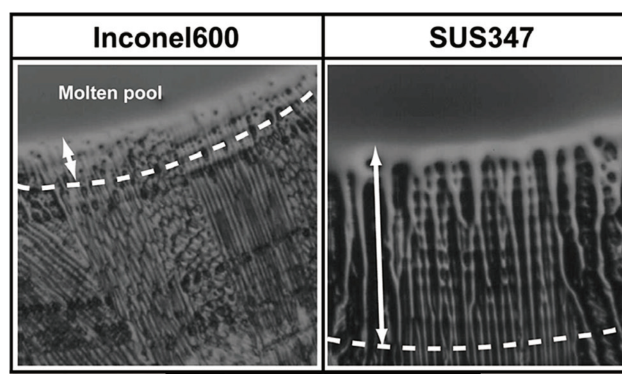

Fig. 19 — Frontlighting with a metal-halide source of weld pool solidification in Inconel 600 and AISI 347 stainless steel when welding with a 2 kW Nd:YAG fiber laser. Optics in this case used microscope lenses (Refs. 57–59).

Frontlighting

Frontlight imaging works by adding supplementary light to the welding region facing the high-speed camera. This technique can reveal additional detail in regions emitting low amounts of radiation, such as the base material, welding electrode, and cooler regions of the weld pool. Successful frontlighting techniques require the reflected light intensity to be greater than the emitted arc and weld pool radiation. The efficiency of such a setup is low due to the scattering of the light in many directions. Therefore, a high-power output frontlight or a pulsed laser system synchronized with the high-speed camera are often required.

This technique is ideally suited to study metal transfer and weld pool and slag movements across a variety of welding processes. The addition of light to regions of low emitted intensity, such as the weld pool or filler wire, can provide more information on weld pool flow velocity, powder flow in processes such as plasma transferred arc welding and laser cladding, and weld pool oscillations. It can also decrease the large dynamic range in pulsed waveforms or short circuit transfer and illuminate the weld pool while the arc is extinguished. Light sources can be in the visible spectral or the invisible range (typically near IR) as long as the camera is sensitive in this region.

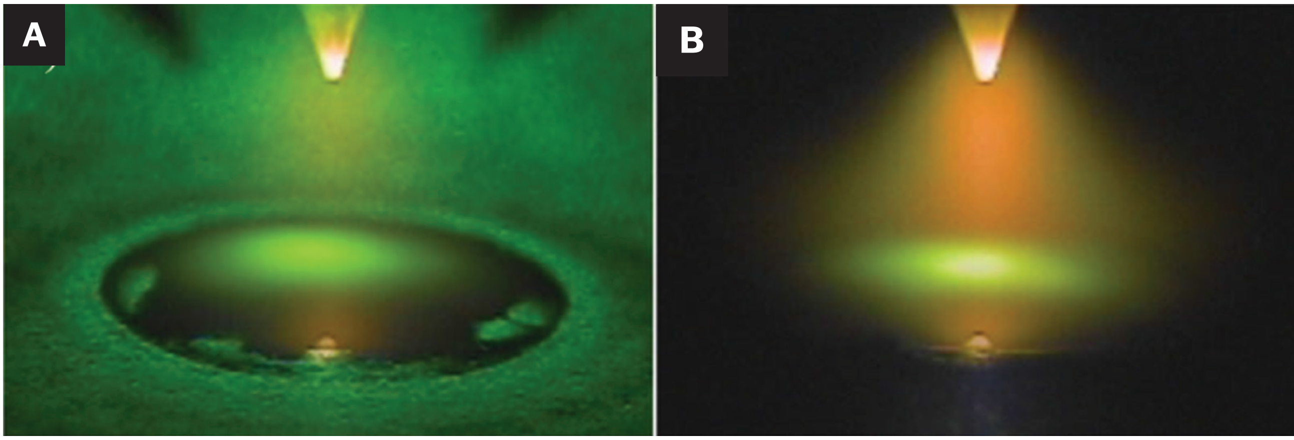

Fig. 20 — Laser frontlighting with NBP filter (A), and natural radiation lighting with the same NBP (B) of GTAW in argon (Ref. 81).

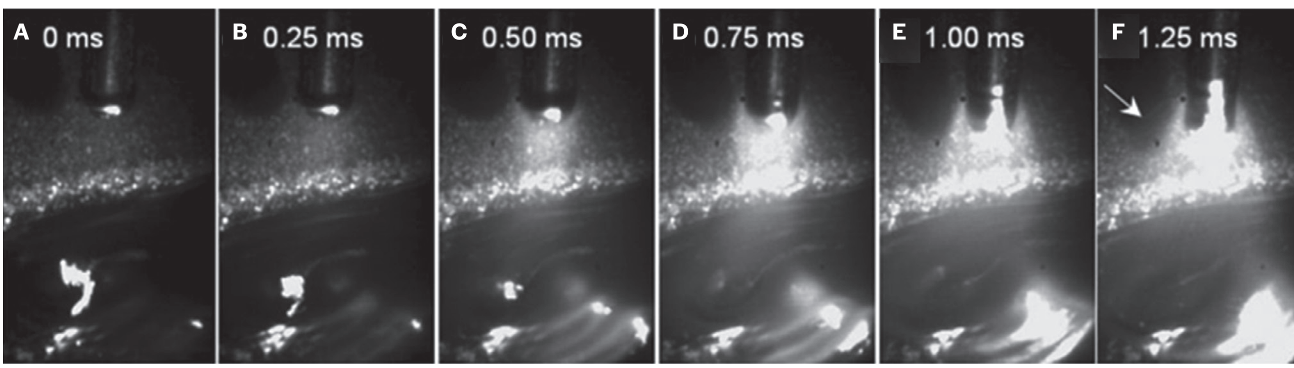

Fig. 21 — Laser frontlighting with a 23 W, 930 nm laser and 930 ± 8.5 nm NBP filter of pulsed GMAW of 5356 aluminum in pure Ar (Ref. 82).

The selection of an appropriate incident light wavelength to avoid overlapping with the spectral peaks of the welding process lowers the incident light power requirements. Utilization of filters, particularly narrow-bandpass, tailored to the incident light source, can eliminate extraneous light and enable the incident light to overpower the emitted arc light in that spectral range. The use of an NBP tailored to the light source also eliminates other molten metal radiation and arc spectral lines. A minor drawback of frontlighting is the formation of specular highlights on reflective surfaces, such as the molten droplets and the weld pool. Specular highlights appear as localized, saturated bright highlights.

Broad Spectrum Frontlighting

Frontlighting with halogen, xenon, LED, or metal-halide light sources is very difficult because of these sources' broad spectrum and consequent high power density requirements. While the visible light sources listed previously are available in high power outputs, the power at specific spectral peaks is much lower.

Collimation of the light source to the region of interest focuses the light and improves the likelihood of overpowering the arc. The light source must be placed near the same line as the high-speed camera to limit the number of shadows in the image. Direct frontlighting, however, produces little discernible detail due to low contrast in the image. An angle of 10–45 deg from the camera direction typically provides appropriate contrast and detail.

Setup for Broad Spectral Frontlighting

The equipment for visible light frontlighting is relatively straightforward. In general, the frontlight's power output has to be high (hundreds of watts and above) and be focused on the region of interest. Using an NBP filter at a characteristic spectral peak reduces extraneous light from the arc and molten metal. If the region of interest has low reflectance, the maximum frame rate might be low because of the exposure times needed. The cost of visible light frontlighting equipment and peripherals is relatively inexpensive and, at the time of publication, could be set up for under $2000.

Examples of Welding Imaging Using Broad-Spectral Frontlighting

Yudodibroto extensively used halogen frontlighting with an ND filter to study the effect of pulsing parameters on weld pool oscillations in autogenous GTAW, cold wire GTAW, and GMAW, as shown in Figs. 17 and 18 (Ref. 55). In Fig. 18,

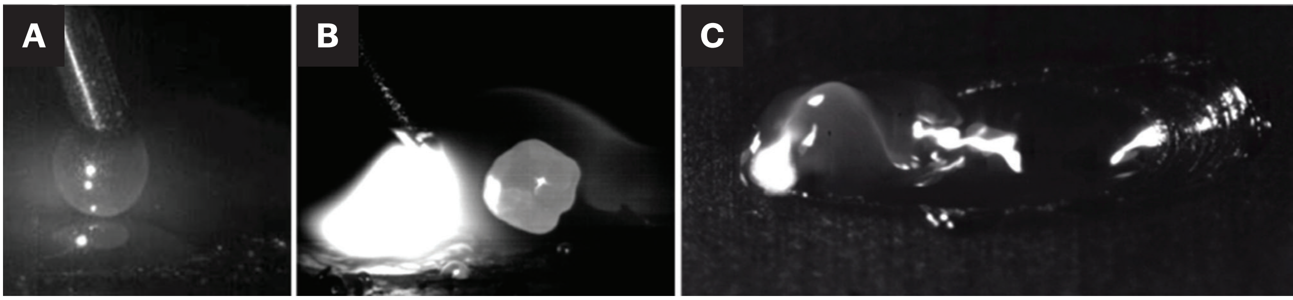

Fig. 22 — Laser frontlight images of: A — GMAW in short-circuit of steel with band pass filter (Ref. 86); B — GMAW in free-flight of steel in Ar-20%CO_2 with 808 nm laser and band pass filter (Ref. 84); C — LBW of stainless steel with a 1.5 kW laser (Ref. 87).

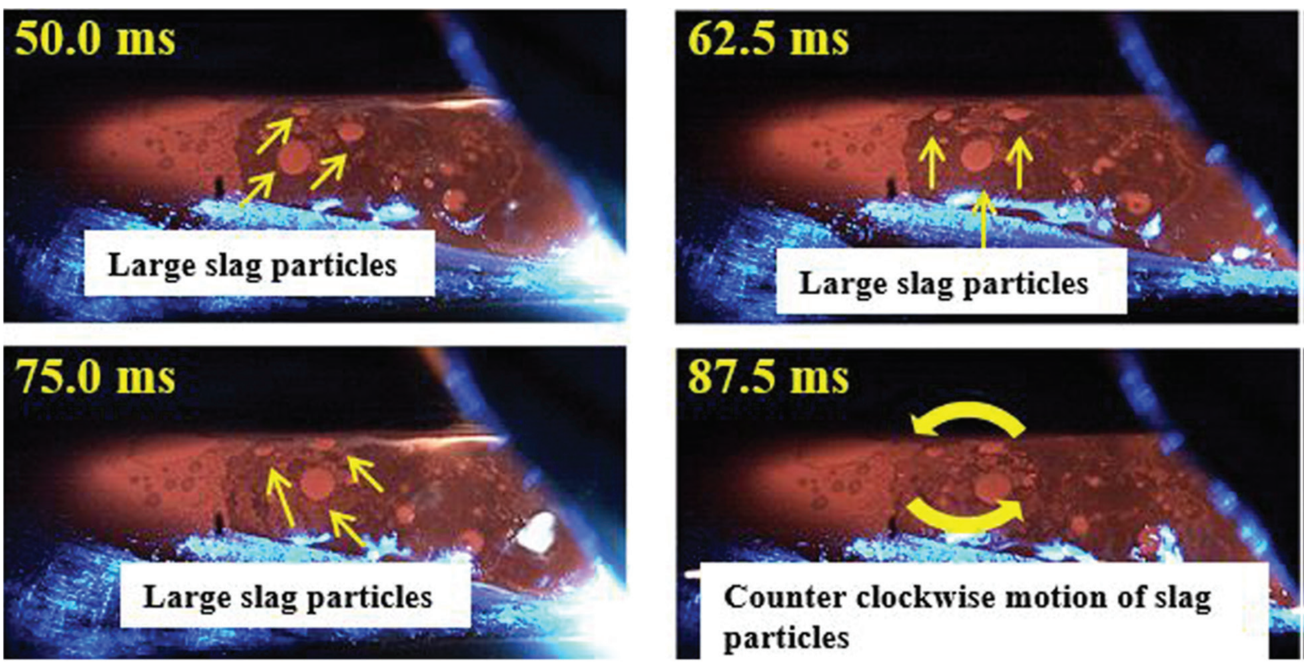

Fig. 23 — LED front lighting of weld pool flow pattern and slag formation. Frame rate was 4000 fps (Ref. 88).

it can be seen how the arc overpowers the frontlighting at 3.0 ms. Wagner et al. employed four 250 W halogen lights with ND filters to observe Mg-alloy GMAW metal transfer (Ref. 56). The low reflectance and power of the halogen frontlighting did not overpower the arc, and the weld pool surface underneath was not visible to the camera during the background or peak current pulse periods. Figure 19 shows metal-halide frontlighting to observe weld pool solidification with microscope lenses and 650 nm bandpass filters at 500 frames per second during Nd:YAG fiber laser welding (Refs. 57–59).

Narrow-Spectrum Frontlighting

Narrow-spectrum frontlighting works on the same principle as broad-spectrum frontlighting. It employs collimated monochromatic LED light sources or lasers to target the beam in a small area. The narrow spectrum enables the use of NBP filters and much lower power sources, producing clear images of the metal droplets, electrodes, and weld pool. The emitter wavelength must be within the sensitivity range of the camera sensor and away from arc spectral lines. Frontlighting with narrow-spectrum light sources, particularly lasers, provides more flexibility to overpower the arc in various welding processes and shielding gases than visible light frontlighting. Furthermore, a narrow-spectrum lighting system capable of frontlighting can also be used as a backlight system, whereas the reverse is not true due to insufficient power outputs.

Using a laser to illuminate a region of interest extends beyond high-speed videography; for example, the laser light can be used to image the weld pool surface contour in real time. In this technique, a pattern of laser light is projected onto the weld pool surface, and reflections on the molten surface are captured on a nearby surface, providing sufficient data to reconstruct the free surface of the weld pool in 3D (Refs. 60–79).

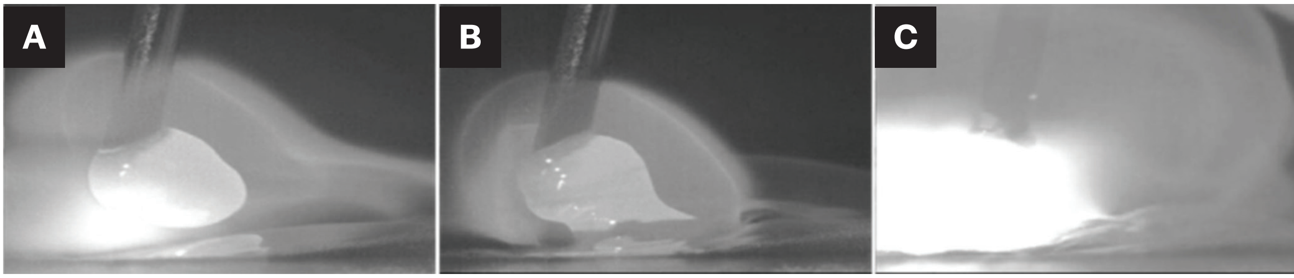

Fig. 24 — Laser frontlighting of GMAW in short circuit: A — Background current during droplet formation; B — short-circuit and droplet transfer; C — arc reestablishment, with high arc currents overexposing the image.

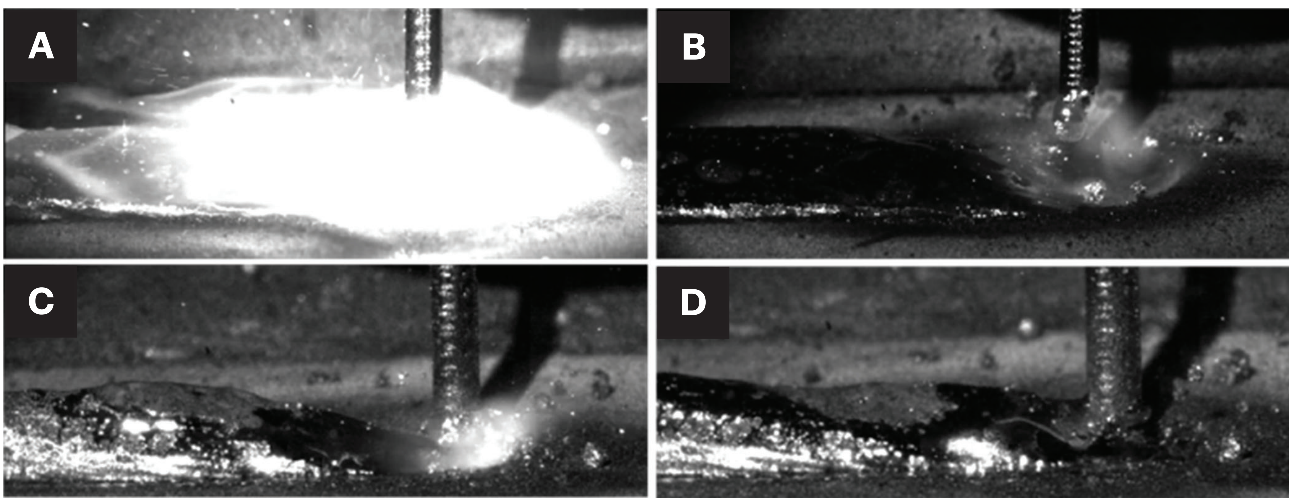

Fig. 25 — Laser frontlighting of GMAW of Ni-WC in Ar-2%O_2. Free flight (A, B), and short circuit (C, D). Exposure time in A was 100 µs, resulting in overexposure. Exposure 1 µs in B, C, and D (Ref. 91).

Setup for Narrow-Spectrum Frontlighting

The equipment required for laser frontlighting is similar to that used in laser backlighting. Laser frontlighting systems incorporate a laser, focusing optics, and an NBP filter centered on the laser's wavelength.

The power requirements for a successful high-speed video laser frontlighting system are much higher than those for laser backlighting. Lower power lasers, such as those below approximately 100 W of instantaneous power, are suitable for lower frame rate imaging (< 4000 fps) where exposure times provide sufficient collection time to form a properly exposed image. Lasers above approximately 100 W of instantaneous power are required when imaging at high frame rates (> 10,000 fps) or when short exposure times are essential to freeze fast-moving objects.

Commercially available lasers of sufficient power are available with continuous pulsed laser outputs. Continuous wave lasers output a constant light intensity and can be costly at high power outputs. Pulsed laser diodes function by pulsing the power supply and the laser diode, increasing the instantaneous power output of the laser system.

Synchronization of the laser pulses with the high-speed camera shutter ensures that the laser pulses occur when the shutter is open. With few commercially available systems, high-power requirements and potential synchronization equipment can be costly. A current commercial system, such as the Cavitar CAVILUZ HF system, features an 810 nm 500 W peak power pulsed laser diode with a 2% duty cycle and pulse durations of 0.1–10 µs [Ref. 80]. The high power outputs and short laser pulse durations allow for frame rates of 100,000 fps. System costs for a complete laser frontlighting system capable of illuminating various welding processes at high frame rates can exceed $40,000, not including the cost of the high-speed camera. Using a laser of this power (often a Class 4) requires special laser safety considerations, especially as these lasers often operate at wavelengths that are invisible to the human eye.

Examples of Welding Imaging Using Narrow-Spectrum Frontlighting

The effect of adding a high-power laser frontlight to overpower the welding arc in GTAW is shown in Fig. 20 (Ref. 81). The weld pool is visualized clearly along with the tungsten electrode in Fig. 20A. For comparison, the same weld is visualized using only natural radiation lighting in Fig. 20B.

When applied to a consumable electrode process, narrow-spectrum frontlighting can provide clear and informative images with short exposure times to freeze motion. In Fig. 21, a 23 W 930 nm laser frontlight was used to illuminate pulsed GMAW welding with aluminum filler wire

(Ref. 82). The lower frame rates and low argon and molten metal spectral intensities at 930 nm allow a lower power continuous wave laser to frontlight the welding process.

Figures 22A and B contain additional sample images during short-circuit and globular transfer in GMAW using steel electrodes (Refs. 83, 84). Narrow-spectrum frontlighting can be applied to analyzing welding defects such as humping, where the low emitted intensity of the weld pool may not provide sufficient light to properly image the region. Nguyen et al. studied the humping phenomenon in high current and fast travel speed GMAW using a 337 nm pulsed N_2 laser with an NBP filter (Ref. 85). Abdullah et al. compared types of lasers when imaging the GTAW process (Ref. 43).

Ahsan et al. used a monochromatic LED light source to illuminate the weld pool area and study the slag formation and weld pool flow (Ref. 88). The authors blocked the arc region with an unspecified mechanical device that avoided overexposure of the images and reduced the required power of the light source to illuminate the region of interest. Samples of the resulting images are included in Fig. 23, in which the mechanical device can be seen as a triangle in the top right corner of the images, with a fine blue line remaining from the arc emissions. The overexposed bottom right corner in the image at 75.0 ms indicates that, without the blocking device, the arc emissions would have overpowered the LED illumination.

Insufficient emitter power when frontlighting can result in images with overexposed arc regions. Overexposure is typical during higher arc currents, such as those observed during pulsed metal transfer or the arc reignition period of short circuit transfer. The saturation of the camera sensors can prevent the imaging of the molten droplet or weld pool. Figure 24 contains sample images of overexposure from low-power laser frontlighting. The effect of saturation can also be seen in Wu et al., who used a non-specified diode laser in conjunction with a 500 ± 5 nm BP filter to capture metal transfer and fluid flow in the weld pool in paraxial hybrid keyhole plasma arc welding and pulsed gas metal arc welding (Refs. 89, 90). During the initial arc ignition of the trailing GMAW torch, the arc overpowered the illuminating laser, especially during connective arc patterns, and the metal transfer was visible only once the arc current dropped and the arcs separated or the GMAW arc extinguished.

Figure 25 shows high-speed images taken with a Cavitar CAVILUX HF system, demonstrating the ability of a high-power laser frontlighting system to eliminate the bright arc during free-flight globular and short-circuit transfer of tubular Ni-WC wire GMAW hardfacing overlays for wear-resistant applications (Ref. 91).

Frontlighting with a narrow-spectrum emitter is also one of the best ways to observe laser welding. Features of interest during laser welding (e.g., keyhole formation) are often too close to the surface to be properly captured with backlighting techniques. Visible light techniques often involve a broad spectrum, and there might not be enough spectral separation from the welding laser. Choosing an illumination light source of a different frequency than the welding laser, together with an NBP filter, is typically the best approach. Figure 22C contains a sample image of autogenous laser welding on stainless steel (Ref. 87). Kawahito et al. used a 30 W 980 nm diode laser, and Wang et al. and Le Guen et al. used an unspecified laser frontlighting to characterize autogenous laser and laser-GMAW hybrid welding with fiber and Nd:YAG lasers (Refs. 92–94). Chen et al. studied the effect of welding position on weld bead shape during laser-GMAW hybrid welding with a laser frontlighting system (Ref. 95). Phaoniam et al. and Liu et al. characterized the hot-wire laser welding process using 980 nm and 532 nm laser frontlight sources for fiber and Yb:YAG lasers, respectively (Refs. 96, 97). Zhang and Gao placed a 25 W 980 nm laser diode source 45 deg relative to the high-speed camera equipped with a 960–990 nm BP filter to image the 1030 nm disk laser weld pool (Ref. 98).

A special case of narrow-spectrum frontlighting is weld vision camera systems that include built-in laser illumination and a tailored filter system. Such systems include a Cavitar welding camera (Ref. 99) and are primarily intended for machine vision and process monitoring, similar to their non-illuminated counterparts (Ref. 100). Typical frame rates are approximately 70 fps, with some ability to increase it up to approximately 500 fps at lower resolutions via sensor cropping.

Summary of Advantages and Disadvantages

The most important advantage of frontlighting is that the intensity of reflected light can overcome the radiation from the arc. This is especially relevant in processes with a high dynamic range of light emission, such as GMAW in short-circuit metal transfer. Frontlighting is unique in providing a detailed image of the surfaces involved, especially of molten metal. Another advantage of frontlighting is to achieve enough light when the fast frame rates allow for short exposures, but the process does not emit much radiation (for example, laser cladding).

The disadvantages of frontlighting are the need for additional equipment compared to natural radiation lighting. Typically, frontlighting is pulsed (strobe lighting; e.g., Cavitar system) to accommodate the high intensity of illumination during a frame while also keeping a lower average intensity of illumination that requires less powerful light sources (e.g., lower power lasers). Strobe lighting involves synchronization between the light source and the camera, which must be taken into account at the time of equipment selection, as some cameras are incompatible with some light sources. When coupling data acquisition with strobe illumination, the challenge of synchronization is even higher. Another disadvantage of frontlighting is that when the arc is only partially overcome, the visible shape of the arc is influenced by the lighting parameters; thus, conclusions about arc shape, size, or attachment are affected by lighting conditions.

The advantages of backlighting are the ability to overcome the arc and produce images with a large contrast ratio that can be more easily captured than with front or natural light illumination. This approach also enables the use of cameras of lower dynamic range. The above reasons made backlighting a popular choice with film cameras. Because backlighting is aimed directly at the camera (not reflected as in the case of frontlighting), lower power and more inexpensive light sources can overcome the arc; strobing is also seldom used. Small amounts of backlighting (that do not saturate the light and dark areas) can provide additional details that are hard to capture with natural radiation lighting, such as a silhouette of the wire in the metal transfer of GMAW.

The main disadvantage of backlighting is that it only provides a silhouette without information about surface features or the arc. Collimation of the laser source, lenses, and camera can be challenging in some cases, with lasers; interference can create visual artifacts such as bands or "speckles." When using x-ray imaging, backlighting is the only lighting technique possible. The main application of backlighting with optical cameras is for metal transfer in wire-based processes.

Broad-spectrum light sources are less expensive than narrow-spectrum light sources (typically lasers); however, narrow-spectrum light sources have the advantage of preserving their light intensity when using narrow-bandpass filters, which are very effective at eliminating the broad radiation from the arc. The disadvantages of narrow-spectrum light sources include the formation of interference patterns in backlighting.

Conclusions

Two of the most common techniques of high-speed imaging of welding have been reviewed in depth: backlighting and frontlighting. For both techniques, broad and narrow-spectrum lighting were discussed (lasers in the case of backlighting). In all cases, detailed descriptions of appropriate setups were provided together with examples of published practical implementations. The welding processes addressed include LBW, GTAW, GMAW, FCAW, and SAW.

Frontlighting is especially useful for processes with high dynamic range when information about the arc, such as short-circuit metal transfer in GMAW, is of secondary importance. Another important application of frontlighting is to reveal surface features in molten metal. Backlighting is less commonly used with modern digital cameras because it provides only a silhouette of the target phenomenon without information about surface features or the arc. Small amounts of backlighting can be complementary to natural radiation lighting to highlight features that emit insufficient light, such as the electrode extension in wire-based processes. Narrow-spectrum sources such as lasers are especially useful in combination with narrow-bandpass filters to eliminate natural or spurious sources of radiation.

The practical implementations reviewed in this paper, together with those for natural radiation lighting in Part 3 and the fundamental concepts and quantitative guidelines provided in Part 1, should enable welding researchers to select the proper equipment, accessories, and parameters for high-speed imaging of a vast variety of phenomena in arc welding, laser welding, and associated processes such as additive manufacturing or cutting.

Acknowledgments

The authors gratefully acknowledge support from the Natural Sciences and Engineering Research Council of Canada (NSERC), Prairies Economic Development Canada (PrairiesCan), CWB Welding Foundation, and in-kind contributions of FLIR, Lincoln Electric, and Miller Electric. Productive conversations with and expertise from Eduardo Alvarez Rocha, Dr. Ivan Pigozzo, and Daniele Calista, along with editing help from Jay Kahar and Aaryan Kumar, are also acknowledged.

References

1. Romero, E., Chapuis, J., Bordreuil, C., Soulie, F., and Fras, G. 2013. Image processing and geometrical analysis for profile detection during pulsed gas metal arc welding. *Proceedings of the Institution of Mechanical Engineers, Part B: Journal of Engineering Manufacture* 227: 396–406. DOI: 10.1177/0954405412470420

2. Chapuis, J., Romero, E., Soulie, F., Bordreuil, C., and Fras, G. 2013. Behaviour of spreading molten metal drops deposited by fusion. *Experimental Thermal and Fluid Science* 48: 29–36. DOI: 10.1016/j.expthermflusci.2013.02.005

3. Nakamura, T., Hiraoka, K., and Zenitani, S. 2008. Improvement of MIG welding stability in pure Ar shielding gas using small amount of oxygen and coaxial hybrid solid wire. *Science and Technology of Welding and Joining* 13: 25–32. DOI: 10.1179/174329307X249289

4. Nakamura, T., and Hiraoka, K. 2011. Effect of coaxial welding wire structure on arc instability in argon shielding gas. *Science and Technology of Welding and Joining* 16: 717–721. DOI: 10.1179/1362171811Y.0000000068

5. Wong, Y.-R., and Ling, S.-F. 2014. An investigation of dynamical metal transfer in GMAW–effects of argon shielding gas. *Journal of Materials Processing Technology* 214: 106–111. DOI: 10.1016/j.jmatprotec.2013.08.003

6. Trinh, N. Q., Le, K. D., Tashiro, S., Suga, T., Sasakura, S., Fukuda, K., Murphy, A. B., Van Bui, H., and Tanaka, M. 2024. Optimization of metal transfer in rutile flux-cored arc welding through controlled CO_2 concentration in argon–CO_2 shielding gas. *Journal of Manufacturing Processes* 124: 590–603. DOI: 10.1016/J.JMAPRO.2024.06.047

7. Pickin, C. G., Williams, S. W., and Lunt, M. 2011. Characterisation of the cold metal transfer (CMT) process and its application for low dilution cladding. *Journal of Materials Processing Technology* 211: 496–502. DOI: 10.1016/j.jmatprotec.2010.11.005

8. Chen, H. M., and Wu, S. J. 2012. Effect of arc length on weld appearance and metal transfer in twin-wire GMAW process. *Advanced Materials Research* 472–475: 1279–1282. DOI: 10.4028/www.scientific.net/AMR.472-475.1279

9. Guo, N., Han, Y. F., Jia, C. B., and Du, Y. P. 2011. Effects of wire rotating frequency on metal transfer process in rotating arc narrow gap horizontal GMAW. *Advanced Materials Research* 189–193: 3395–3399. DOI: 10.4028/www.scientific.net/AMR.189-193.3395

10. Praveen, P., Kang, M. J., and V Prasad, Y. K. D. 2006. Behaviour of metal transfer modes in pulse gas metal arc welding of aluminum. *Advanced Materials Processing Technologies Conference* 2006.

11. Zhang, S., Wu, D., Cao, M., and Zou, Z. 2009. Metal transfer modes of twin-wire indirect arc welding. F*rontiers of Materials Science* 3: 426–433. DOI: 10.1007/s11706-009-0056-6

12. Zheng, S. M., Gao, H. M., and Liu, X. 2011. Metal transfer characteristics of GMAW with strip electrode. *Science and Technology of Welding and Joining* 16: 586–591. DOI: 10.1179/1362171811Y.0000000046

13. Chen, M. A., Jiang, Y. N., and Wu, C. S. 2013. Effect of current waveform on metal transfer in controlled short circuiting gas metal arc welding. *Advanced Materials Research* 718–720: 202–208. DOI: 10.4028/www.scientific.net/AMR.718-720.202

14. Feng, J., Zhang, H., and He, P. 2009. The CMT short-circuiting metal transfer process and its use in thin aluminium sheets welding. *Materials & Design* 30: 1850–1852. DOI: 10.1016/j.matdes.2008.07.015

15. Wang, J., Wu, D., Liao, P., Tian, C. Y., Li, M. Q., and Feng, J. C. 2013. Metal transfer and arc behaviour of novel consumable and non-consumable electrode indirect arc droplet welding. *Science and Technology of Welding and Joining* 18: 261–270. DOI: 10.1179/1362171812Y.0000000103

16. Kim, C. H., Ahn, Y. N., and Lee, K. B. 2012. Droplet transfer during conventional gas metal arc and plasma-gas metal arc hybrid welding with Al 5183 filler metal. *Current Applied Physics* 12: S178–S183. DOI: 10.1016/j.cap.2012.03.001

17. Lenivkin, V. A., Kiselev, D. V., and Parshin, S. G. 2013. Non-uniform melting of the electrode at supercritical current in argon. *Welding International* 27: 281–286. DOI: 10.1080/09507116.2012.715911

18. Liu, H.-Y., Li, Z.-X., Li, H., and Shi, Y.-W. 2008. Study on metal transfer modes and welding spatter characteristics of self-shielded flux cored wire. *Science and Technology of Welding and Joining* 13: 777–780. DOI: 10.1179/174329308X380354

19. Soderstrom, E. J. 2009. Gas metal arc-welding electrode heat-and-mass transfer mechanisms. PhD diss., Colorado School of Mines.

20. Allemand, C. D., Schoeder, R., Ries, D. E., and Eagar, T. W. 1985. A method of filming metal transfer in welding arcs. *Welding Journal* 64(1): 45–47.

21. Zhang, Y. M., Eagar, L., and Kovacevic, R. 1998. Active metal transfer control by monitoring excited droplet oscillation. *Welding Journal* 77(9): 388-s to 395-s.

22. Zhang, Y. M., and Li, P. J. 2001. Modified active control of metal transfer and pulsed GMAW of titanium. *Welding Journal* 80(2): 54-s to 62-s.

23. Zhang, Y. M., Eagar, L., and Walcott, B. L. 2002. Robust control of pulsed gas metal arc welding. *Journal of Dynamic Systems, Measurement, and Control* 124: 281–289. DOI: 10.1115/1.1470173

24. Subramaniam, S., White, D. R., Jones, J. E., and Lyons, D. W. 1998. Droplet transfer in pulsed gas metal arc welding of aluminum. *Welding Journal* 77: 458-s to 464-s.

25. Soderstrom, E. J., and Mendez, P. F. 2008. Metal transfer during GMAW with thin electrodes and Ar-CO2 shielding gas mixtures. *Welding Journal* 87(5): 124-s–133-s.

26. Soderstrom, E., Scott, K., and Mendez, P. 2011. Calorimetric measurement of droplet temperature in GMAW. *Welding Journal* 90(4): 77-s to 84-s.

27. Jones, L. A., Eagar, T. W., and Lang, J. H. 1998. Images of a steel electrode in Ar-2%O2 shielding during constant current gas metal arc welding. *Welding Journal* 77(4): 135-s to 141-s.

28. Scotti, A., Ponomarev, V., and Lucas, W. 2012. A scientific application oriented classification for metal transfer modes in GMA welding. *Journal of Materials Processing Technology* 212: 1406–1413. DOI: 10.1016/J.JMATPROTEC.2012.01.021

29. Scotti, A., and Ponomarev, V. 2014. *Soldagem MIG/MAG: melhor entendimento, melhor desempenho*, 2nd edition. Sao Paulo, Brazil: Artliber.

30. Soderstrom, E., Scott, K., and Mendez, P. 2011. Calorimetric measurement of droplet temperature in GMAW. *Welding Journal* 90(4): 77-s to 84-s.

31. Jones, L. A., Eagar, T. W., and Lang, J. H. 1998. Images of a steel electrode in Ar-2%O2 shielding during constant current gas metal arc welding. *Welding Journal* 77(4): 135-s to 141-s.

32. Yuan-mei, W., Shi-sheng, H., Jia-xiang, X., and Xiao, L. 2007. Key techniques on design of laser high-speed video system for recording metal transfer in arc welding. *The Eighth International Conference on Electronics Measurements and Instruments*: 900–903.

33. Rhee, S., and Kannatey-Asibu, E. 1992. Observation of metal transfer during gas metal arc welding. *Welding Journal* 71: 381-s to 386-s.

34. Bálsamo, P. S. S., Scotti, A., Vilarinho, L. O., and Vilela, M. 2000. Development of an experimental technique for studying metal transfer in welding: synchronized shadowgraphy. *International Journal for the Joining of Materials* 12: 1–12.

35. Scotti, A., Morais, C. O., and Vilarinho, L. O. 2006. The effect of out-of-phase pulsing on metal transfer in twin-wire GMA welding at high current level. *Welding Journal* 85: 225-s to 230-s.

36. Scotti, A., and Rodrigues, C. E. A. L. 2009. Determination of the momentum of droplets impinging on the pool during aluminium GMAW. *Soldagem & Inspeção* 14: 336–343.

37. Alves de Resende, A., Keocheguerians, F., and Vilarinho, L. O. 2010. The influence of CO2 and O2 content on globular spray transition current when using argon-based blends in GMAW of ER70S-6 wire. *Welding International* 24(8): 593–601. DOI: 10.1080/09507110903568828

38. Abdullah, B. M. 2012. "Monitoring of welding using laser diodes." In *Semiconductor Laser Diode Technology and Applications*, edited by Patil, D. S., 241–262.

39. Liu, S., Liu, F., Zhang, H., and Shi, Y. 2012. Analysis of droplet transfer mode and forming process of weld bead in CO_2 laser–MAG hybrid welding process. *Optics & Laser Technology* 44: 1019–1025. DOI: 10.1016/j.optlastec.2011.10.016

40. Mota, C. P., Machado, M. V. R., Finzi Neto, R. M., and Vilarinho, L. O. 2013. Near-infrared vision system for arc-welding monitoring. *Soldagem & Inspeção* 18: 19–30. DOI: 10.1590/S0104-92242013000100004

41. Rusu, C. C., Mistodie, L. R., and Ghita, E. 2011. Laser shadowgraph system for the electrical arc investigation. *U.P.B. Scientific Bulletin, Series D* 73: 189–198.

42. Wen, Y. M., Huang, S. S., and Liu, G. X. 2011. Testing and analysis of high-speed camera for droplet transition. *Advanced Materials Research* 271–273: 79–83. DOI: 10.4028/www.scientific.net/AMR.271-273.79

43. Abdullah, B. M., Smith, J. S., Lucas, W., Lucas, J., and Malek, F. 2008. Monitoring of TIG welding using laser and diode illumination sources: a comparison study. *2008 International Conference on Electronic Design*, Penang, Malaysia.

44. Zhang, W., Hua, X., Liao, W., Li, F., and Wang, M. 2014. Study of metal transfer in CO_2 laser+GMAW-P hybrid welding using argon–helium mixtures. *Optics & Laser Technology* 56(3): 158–166. DOI: 10.1016/j.optlastec.2013.08.006

45. Mamat, S., Tashiro, S., Tanaka, M., and Yusoff, M. 2018. Study on factors affecting the droplet temperature in plasma MIG welding process. *Journal of Physics D: Applied Physics* 51(13). DOI: 10.1088/1361-6463/aab128

46. Mvola, B., and Kah, P. 2017. Effects of shielding gas control: welded joint properties in GMAW process optimization. *The International Journal of Advanced Manufacturing Technology* 88: 2369–2387. DOI: 10.1007/s00170-016-8936-2

47. Mrňa, L., Pavelka, J., Horník, P., and Hrabovský, J. 2016. Use of schlieren methods to study gas flow in laser technology. *Proceedings of SPIE: The International Society for Optical Engineering*. DOI: 10.1117/12.2257212

48. Qaisrani, M. H., Xian, Y., Li, C., Pei, X., Ghasemi, M., and Lu, X. 2016. Study on dynamics of the influence exerted by plasma on gas

flow field in non-thermal atmospheric pressure plasma jet. *Physics of Plasmas* 23: 063523. DOI: 10.1063/1.4954828

49. Schnick, M., Dreher, M., Zschetzsche, J., Fuessel, U., and Spille-Kohoff, A. 2012. Visualization and optimization of shielding gas flows in arc welding. *Welding in the World* 56: 54–61. DOI: 10.1007/BF03321146

50. Bitharas, I., McPherson, N. A., McGhie, W., Roy, D., and Moore, A. J. 2017. Visualisation and optimisation of shielding gas coverage during gas metal arc welding. *Journal of Materials Processing Technology*. DOI: 10.1016/j.jmatprotec.2017.11.048

51. Siewert, E., Wilhelm, G., Hässler, M., Schein, J., Hanson, T., Schnick, M., and Füssel, U. 2014. Visualization of gas flows in welding arcs by the Schlieren measuring technique: The influence of typical welding parameters on the gas flow for the GTAW, GMAW, and PAW processes. *Welding Journal* 93(1): 1-s to 5-s.

52. Zhang, Y., Jia, C., Zhao, B., Hu, J., and Wu, C. 2016. Heat input and metal transfer influences on the weld geometry and microstructure during underwater wet FCAW. *Journal of Materials Processing Technology* 238: 373–382. DOI: 10.1016/J.JMATPROTEC.2016.07.024

53. Jia, C., Wu, J., Han, Y., Zhang, Y., Yang, Q., and Wu, C. S. 2020. Underwater pulse-current FCAW — Part 1: Waveform and process features. *Welding Journal* 99(5): 135-s to 145-s. DOI: 10.29391/2020.99.013

54. Li, K., Wu, Z., Zhu, Y., and Liu, C. 2017. Metal transfer in submerged arc welding. *Journal of Materials Processing Technology* 244: 314–319. DOI: 10.1016/j.jmatprotec.2017.02.004

55. Yudodibroto, B. M. 2010. Liquid metal oscillation and arc behaviour during welding. Doctorial thesis., Delft University of Technology.

56. Wagner, D. C., Yang, Y. K., and Kou, S. 2013. Spatter and porosity in gas-metal arc welding of magnesium alloys: Mechanisms and elimination. *Welding Journal* 92(12): 347-s to 362-s.

57. Wen, P., Yamamoto, M., Senda, Y., Tamura, T., and Shinozaki, K. 2010. Study on solidification cracking of laser dissimilar welded joints by using in-situ observation and numerical simulation. *Welding in the World* 54: R257–R266.

58. Wen, P., Shinozaki, K., Yamamoto, M., Senda, Y., Tamura, T., and Nemoto, N. 2009. In-situ observation of solidification cracking of laser dissimilar welded joints. *Quarterly Journal of the Japan Welding Society* 27: 134–138.

59. Shinozaki, K., Yamamoto, M., Kawasaki, A., Tamura, T., and Wen, P. 2008. Development of evaluation method for solidification cracking susceptibility of Inconel600/SUS347 dissimilar laser weld metal by in-situ observation. *Materials Science Forum* 580–582: 49–52. DOI: 10.4028/www.scientific.net/MSF.580-582.49

60. Liu, Y., and Zhang, Y. 2013. Control of 3D weld pool surface. *Control Engineering Practice* 21: 1469–1480. DOI: 10.1016/j.conengprac.2013.06.019

61. Liu, Y. K., Zhang, W. J., and Zhang, Y. M. 2013. Estimation of weld joint penetration under varying GTA pools. *Welding Journal* 92(11): 313-s to 321-s.

62. Ma, X., and Zhang, Y. 2013. Reconstruction of three-dimensional gas metal arc weld pool surface from reflected laser pattern. *Journal of Manufacturing Science and Engineering* 135: 1–11. DOI: 10.1115/1.4023374

63. Zhang, W., Wang, X., and Zhang, Y. 2013. Analytical real-time measurement of a three-dimensional weld pool surface. *Measurement Science and Technology* 24: 1–18. DOI: 10.1088/0957-0233/24/11/115011

64. Zhang, W., Zhang, X., Liu, Y., and Zhang, Y. 2013. Robust pattern recognition of three dimensional weld pool surface in gas tungsten arc welding. *2013 IEEE International Instrumentation and Measurement Technology Conference (I2MTC)*, 1652–1657. DOI: 10.1109/I2MTC.2013.6555694

65. Zhang, W. J., Zhang, X., and Zhang, Y. M. 2013. Robust pattern recognition for measurement of three dimensional weld pool surface in GTAW. *Journal of Intelligent Manufacturing*: 659–676. DOI: 10.1007/s10845-013-0825-z

66. Zhang, W., Liu, Y., and Zhang, Y. 2013. Real-time measurement of the weld pool surface in GTAW process. *2013 IEEE International Instrumentation and Measurement Technology Conference (I2MTC)*, 1640–1645. DOI: 10.1109/I2MTC.2013.6555692

67. Liu, Y. K., Chen, S. J., Zhang, W. J., and Zhang, Y. M. 2013. Nonlinear dynamic modelling of weld penetration in gas tungsten arc welding process. *Advanced Materials Research* 658: 292–297. DOI: 10.4028/www.scientific.net/AMR.658.292

68. Wang, Z., Zhang, Y., and Yang, R. 2013. Analytical reconstruction of three-dimensional weld pool surface in GTAW. *Journal of Manufacturing Processes* 15: 34–40. DOI: 10.1016/j.jmapro.2012.08.002

69. Wang, Z., Huang, X., Yang, R., and Zhang, Y. 2012. Measurement of mirror surfaces using specular reflection and analytical computation. *Machine Vision and Applications* 24: 289–304. DOI: 10.1007/s00138-012-0432-6

70. Zhang, W., Liu, Y., Wang, X., and Zhang, Y. M. 2012. Characterization of three-dimensional weld pool surface in GTAW. *Welding Journal* 91(7): 195-s to 203-s.

71. Ma, X., Zhang, Y., Gay, A. M., and Male, A. T. 2012. Image processing for measurement of three-dimensional gas metal arc weld pool surface. *IEEE International Conference on Computer Science and Automation Engineering*, 243–249. Zhangjiajie, China.

72. Ma, X., and Zhang, Y. 2009. Reflection of illumination laser from gas metal arc weld pool surface. *Measurement Science and Technology* 20: 1–8. DOI: 10.1088/0957-0233/20/11/115105

73. Ma, X., and Zhang, Y. M. 2011. Gas metal arc weld pool surface imaging: Modeling and processing. *Welding Journal* 90(5): 85-s to 94-s.

74. Zhang, Y. M., Song, H. S., and Saeed, G. 2006. Observation of a dynamic specular weld pool surface. *Measurement Science and Technology* 17. DOI: 10.1088/0957-0233/17/6/L02

75. Saeed, G., and Zhang, Y. M. 2007. Weld pool surface depth measurement using a calibrated camera and structured light. *Measurement Science and Technology* 18: 2570–2578. DOI: 10.1088/0957-0233/18/8/033

76. Song, H. S., and Zhang, Y. M. 2007. Image processing for measurement of three-dimensional GTA weld pool surface. *Welding Journal* 86(10): 323-s to 330-s.

77. Song, H. S., and Zhang, Y. M. 2008. Measurement and analysis of three-dimensional specular gas tungsten arc weld pool surface. *Welding Journal* 87(4): 85-s to 95-s.

78. Song, H. S., and Zhang, Y. M. 2007. Three-dimensional reconstruction of specular surface for a gas tungsten arc weld pool. *Measurement Science and Technology* 18: 3751–3767. DOI: 10.1088/0957-0233/18/12/010

79. Song, H., and Zhang, Y. 2007. An image processing scheme for measurement of specular weld pool surface. *2nd IEEE Conference on Industrial Electronics and Applications*, 5–10.

80. Cavitar. Welding imaging. Retrieved June 23, 2020, from *cavitar.com/applications/welding-imaging/*

81. Ogawa, Y. 2011. High speed imaging technique Part 1 — high speed imaging of arc welding phenomena. *Science and Technology of Welding and Joining* 16: 33–43. DOI: 10.1179/136217110X12785889549903

82. Wang, J.-B., Nishimura, H., Katayama, S., and Mizutani, M. 2011. Evaporation phenomena of magnesium from droplet at welding wire tip in pulsed MIG arc welding of aluminium alloys.

Science and Technology of Welding and Joining 16: 418–425. DOI: 10.1179/1362171810Y.0000000030

83. Planckaert, J.-P., Djermoune, E.-H., Brie, D., Briand, F., and Richard, F. 2010. Modeling of MIG/MAG welding with experimental validation using an active contour algorithm applied on high speed movies. *Applied Mathematical Modelling* 34: 1004–1020. DOI: 10.1016/j.apm.2009.07.011

84. Feng, J., Li, L., Chen, Y., Lei, Z., Qin, H., and Li, Y. 2012. Effects of welding velocity on the impact behavior of droplets in gas metal arc welding. *Journal of Materials Processing Technology* 212: 2163–2172. DOI: 10.1016/j.jmatprotec.2012.02.016

85. Nguyen, T. C., Weckman, D. C., Johnson, D. A., and Kerr, H. W. 2005. The humping phenomenon during high speed gas metal arc welding. *Science and Technology of Welding and Joining* 10: 447–459.

86. Planckaert, J.-P., Djermoune, E.-H., Brie, D., Briand, F., and Richard, F. 2010. Modeling of MIG/MAG welding with experimental validation using an active contour algorithm applied on high speed movies. *Applied Mathematical Modelling* 34: 1004–1020. DOI: 10.1016/j.apm.2009.07.011

87. Thiel, C., Hess, A., Weber, R., and Graf, T. 2012. Stabilization of laser welding processes by means of beam oscillation. *Proceedings of SPIE - The International Society for Optical Engineering* 8433:26. DOI: 10.1117/12.922403

88. Ahsan, M. R. U., Cheepu, M., Ashiri, R., Kim, T. H., Jeong, C., and Park, Y. D. 2017. Mechanisms of weld pool flow and slag formation location in cold metal transfer (CMT) gas metal arc welding (GMAW). *Welding in the World* 61: 1275–1285. DOI: 10.1007/s40194-017-0489-y

89. Wu, D., Tashiro, S., Wu, Z., Nomura, K., Hua, X., and Tanaka, M. 2020. Interactive phenomena in hybrid KPAW–GMAW-P. *Welding Journal* 99(5): 146-s to 155-s. DOI: 10.29391/2020.99.014

90. Wu, D., Tashiro, S., Wu, Z., Nomura, K., Hua, X., and Tanaka, M. 2020. Analysis of heat transfer and material flow in hybrid KPAW-GMAW process based on the novel three dimensional CFD simulation. *International Journal of Heat and Mass Transfer* 147: 1–14. DOI: 10.1016/j.ijheatmasstransfer.2019.118921

91. Cavitar. 2012. Product demonstration. "Cavitar Cavilux HF" at Canadian Centre for Welding + Joining, Edmonton, Alberta.

92. Kawahito, Y., Matsumoto, N., Abe, Y., and Katayama, S. 2013. Laser absorption characteristics in high-power fibre laser welding of stainless steel. *Welding International* 27: 129–135. DOI: 10.1080/09507116.2011.606151

93. Wang, J., Wang, C., Meng, X., Hu, X., Yu, Y., and Yu, S. 2011. Interaction between laser-induced plasma/vapor and arc plasma during fiber laser-MIG hybrid welding. *Journal of Mechanical Science and Technology* 25: 1529–1533. DOI: 10.1007/s12206-011-0410-3

94. Le Guen, E., Fabbro, R., Carin, M., Coste, F., and Le Masson, P. 2011. Analysis of hybrid Nd:Yag laser-MAG arc welding processes. *Optics & Laser Technology* 43: 1155–1166. DOI: 10.1016/j.optlastec.2011.03.002

95. Chen, Y. B., Feng, J. C., Li, L. Q., Li, Y., and Chang, S. 2013. Effects of welding positions on droplet transfer in CO2 laser–MAG hybrid welding. *The International Journal of Advanced Manufacturing Technology* 68(5–8): 1351–1359. DOI: 10.1007/s00170-013-4926-9

96. Phaoniam, R., Shinozaki, K., Yamamoto, M., Kadoi, K., Tsuchiya, S., and Nishijima, A. 2013. Development of a highly efficient hot-wire laser hybrid process for narrow-gap welding—welding phenomena and their adequate conditions. *Welding in the World* 57: 607–613. DOI: 10.1007/s40194-013-0055-1

97. Liu, W., Liu, S., Ma, J., and Kovacevic, R. 2014. Real-time monitoring of the laser hot-wire welding process. *Optics & Laser Technology* 57: 66–76. DOI: 10.1016/j.optlastec.2013.09.026

98. Zhang, Y., and Gao, X. 2013. Analysis of characteristics of molten pool using cast shadow during high-power disk laser welding. *The International Journal of Advanced Manufacturing Technology* 70(9–12). DOI: 10.1007/s00170-013-5442-7

99. Cavitar. Cavitar Welding Camera. Retrieved January 18, 2022, from *cavitar.com/product/cavitar-welding-camera/.*

100. Xiris Inc. Xiris Solutions for Weld Inspection and Monitoring. Retrieved from *xiris.com*.

GREGOR GÖTT is with the Leibniz Institute for Plasma Science and Technology, **STUART DAN GUEST**, **GOETZ DAPP**, **JULIEN CHAPUIS**, and **PATRICIO MENDEZ** (*pmendez@ualberta.ca*) are with the University of Alberta, Donadeo Innovation Centre for Engineering, Edmonton, Alberta, Canada.